Article

Intelligent System for Analysis and Monitoring of Flood Embankments Based on Electrical Impedance Tomography, Machine Learning and Internet of Things

Tomasz Rymarczyk[1,2,*], Edward Kozłowski[3], Grzegorz Kłosowski[3]

[1] University of Economics and Innovation in Lublin, Poland; tomasz@rymarczyk.com
[2] Research & Development Centre Netrix S.A., Lublin, Poland
[3] Faculty of Management, Lublin University of Technology, Lublin, Poland; g.klosowski@pollub.pl, e.kozlovski@pollub.pl
[*] Correspondence: tomasz@rymarczyk.com

Abstract: The article presents a non-destructive test system based on electrical impedance tomography for monitoring flood embankments. The technology of cyber-physical systems and the Internet of Things with the use of electrical impedance tomography enables real-time monitoring of flood embankments. This solution provides a visual analysis of damage and leaks, which allows for quick and effective intervention and possible prevention of danger. A dedicated solution based on the IT structure, dedicated laboratory models and a dedicated measurement system with various types of sensors and machine learning algorithms for image reconstruction has been developed. The system includes specialized intelligent devices for tomographic measurements. The application contains the analysis of anomalies occurring in the structure of the object as a result of damage or danger and breaking the shaft during the flood. The presented solution enables ongoing monitoring of objects by collecting measurement results, forecasts and simulations. The main advantage of the proposed system is the spatial ability to analyse shafts, high accuracy of imaging and high speed of data processing. The use of tomographic techniques in conjunction with image reconstruction algorithms allow for non-invasive and very accurate spatial assessment of humidity and damages of flood embankments. The presented results show the effectiveness of the presented research.

Keywords: inverse problem; electrical impedance tomography; machine learning; flood embankment; internet of things

1. Introduction

In this article the results of research of a monitoring system based on electrical impedance tomography (EIT) with special measuring sensors for testing flood embankments have been presented. Floods cause huge damage and are the cause of many tragedies. The rapid increase in the amount of water in the rivers between the embankments causes pressure of water, erosion of the upper surface of the embankment, leaks and breakage of the embankment. Therefore, the proposed solution is of great importance as a system for maintaining and monitoring flood embankments. The most common flood embankment is a structure made of material found in the vicinity of the river. Despite large advances in the design of embankments, unexpected changes in the structure of objects may occur.

Currently, continuous monitoring of flood embankments is difficult due to their large size. Internet of Things (IoT) gives great opportunities to build distributed systems, using wireless devices,

mobile devices and sensor networks. IoT connects various devices on the network. A service-oriented architecture (SOA) can be used to service the Internet. This architecture is used in areas such as cloud computing or wireless sensor network (WSN). The IoT architectural project should have the possibility of extending, scalability, modularity and interoperability of cooperating devices. IoT as a cyber-physical system (CPS) integrates various devices equipped with detection, identification, processing, communication and network functions [1]. In order to enable devices processing data located on the edge of the network, aimed at improving the user experience and service resilience in the event of failure, fog/edge computing is applied. Using a distributed architecture can provide faster response and better service quality. CPS can effectively integrate both cyber and physical components through the integration of modern technologies, changing the methods of interaction between the human, cybernetic and physical worlds. This solution is used to analyse measurement data and send feedback commands, ensuring system operation in the desired states [2]. The massive data generated by the IoT is used to analyse and explore data (including hidden information) with the use of machine learning. In order to achieve better performance, the algorithms used should be modified to ensure optimal application to large data sets. Using IoT and relevant technologies, it can integrate classic networks with networked devices. In each solution the basic challenge is to study large amounts of data and extract useful information or knowledge related to data extraction and intelligence algorithms. To make the right decisions, data mining technologies integrate with IoT technologies to support and optimize the system [3]. It can use a CPS-based solution for online processing of tomography data streams. Information on such data can be incorporated into automated decision systems for IoT applications. It has been proven that computer intelligence methods are capable of solving very complex tasks, such as processing natural human language, but require large training data bodies. Current monolithic tomographic systems provide limited support for computer intelligence methods, given the limited space and time of their computational components. To gain robust support for automated decision systems, a distributed computing cloud architecture for computing tomographic data streams online has been presented and analysed [4].

Embankments are built from compacted material are an integral part of every flood protector. Many shafts are in poor condition; therefore, flood protection will be tested with increasing regularity. Current methods of visual identification of cracks and soak in flood embankments are insufficient. Defects cannot be discovered without excavation, which is quite costly and destructive for the construction of the embankment. Electrical impedance tomography (EIT) is a non-invasive method to assess the structure of the embankment [5]. The EIT is sensitive to the presence of cracks and permeates, which makes it highly effective for monitoring shafts [6]. The monitoring system and flood embankments consists of sensors, IoT nodes, gates and cloud-based services. The nodes communicate with sensors measuring specific parameters. As part of the Internet of Things, all connected devices create a cloud, a smart environment where data can be combined from different devices on a cloud server and analysed using Big Data. IoT combines different technologies, combining individual devices in a network and providing two-way communication. The solution also includes software and services analysing the data provided by the devices, where they are then used in the decision-making process. Monitoring systems of flood embankments are mainly limited to visual and geotechnical tests. Testing on objects is carried out at test points located in a large area. The intelligent monitoring system should examine the state of flood embankment in terms of damage and answering. Sensor networks should be located on the site and investigate specific geophysical and hydrological phenomena. The architecture of the system consists of measuring devices, sensors (IoT) and application (services) in the cloud. Data collected from measurements are analysed using appropriate algorithms. This way of approaching allows for sending appropriate messages about the flood hazard. The system can react automatically to observed changes, e.g. by increasing the frequency of measurements [7]. An example solution of levee monitoring for collecting data from the reference and experimental control and measurement network is presented in [8]. It uses a range of pressure and temperature sensors and fiber optic technologies to monitor changes in the body of the embankment.

Preprints (www.preprints.org) | NOT PEER-REVIEWED | Posted: 20 August 2018 doi:10.20944/preprints201808.0346.v1

Geophysical methods are widely used in geotechnics and in environmental research. They contain measurement methods and imaging of tested objects [9]. Research shows how integrated technologies can be used to study complex anisotropic areas. The advantage of geophysical methods is their non-invasive nature and relatively low costs. They can be used for rapid imaging in a variety of materials, including soil. Each hydrological facility requires constant and safe monitoring to keep track of possible threats. In such objects there are complex physical processes related to the impact of water on them.

Methods of geophysical research most commonly used:

- ground penetrating radar (GPR),
- electro-resistance method (ERM),
- seismic method (SM),
- electromagnetic method (EM),
- gravimetric method (GM).

Each of the mentioned methods uses a different geophysical phenomenon. The use of a particular method depends on the expected results. Measurements are made using specialized measuring devices. The obtained results require further analysis through the processing of signals and their appropriate interpretation, mainly in the form of profile or cross-section imaging.

Geophysical measurements using the seismic method are based on the measurement and analysis of artificially generated seismic waves in the studied area. The measurement is based on changes in the elasticity parameters of the tested medium by transferring vibrations through the medium being tested.

The microgravimetric method is based on the analysis of gravitational changes that are caused by inhomogeneous distribution of rock masses by determining weak areas of the ground. Most often this method locates voids in the examined objects [10].

The analysis of disturbances of the induced electromagnetic field in the centre gives the possibility of locating various objects. The electromagnetic method can be used to detect changes in soil resistance (degree of soil contamination, leakage, detection of objects).

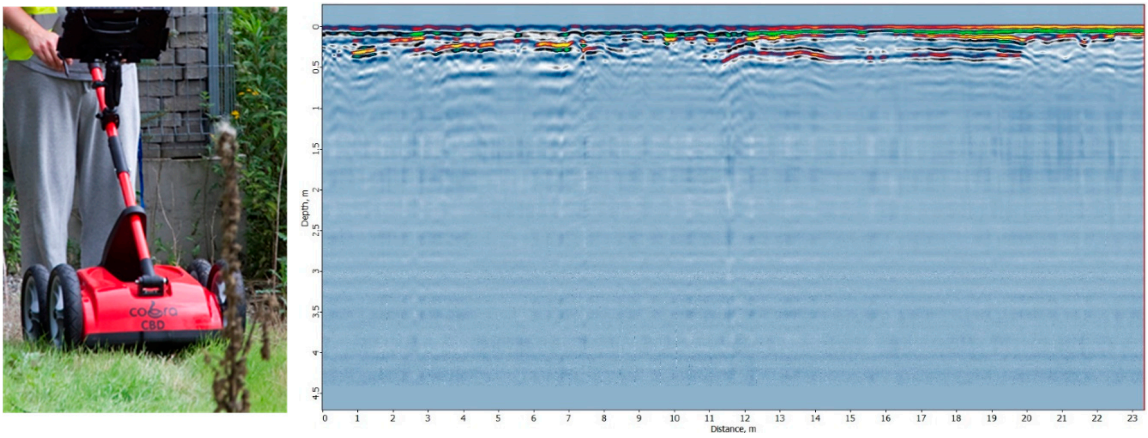

(a) (b)

Figure 1. Ground Penetrating Radar: (a) device during measurements, (b) profile of the subsurface area representation by GPR study

GPR radar method allows analysis of propagation of electromagnetic waves in the tested object [11]. The waves pass through the object causing a break, reflection and diffraction. By analysing the reflected signal, you can determine the location of objects and observe changes in the structure of the tested medium. In GPR electromagnetic waves at frequencies from 50 MHz to 2.5 GHz are transmitted. A radio wave transmitter placed on the surface is used to generate a short pulse of radio waves that penetrate into the subsurface. Part of the energy is transferred to increasing depths, while another part of energy is reflected when it encounters contrast in dielectric properties. The receiver measures the variability of the intensity of the reflected signals over time. The amount of energy

Preprints (www.preprints.org) | NOT PEER-REVIEWED | Posted: 20 August 2018 doi:10.20944/preprints201808.0346.v1

reflected depends on the contrast of the electrical properties encountered by the radio waves. The resulting profile is a representation of the subsurface area. The method is used to detect geological and geotechnical boundaries, voids, subsidence and detection of objects. An exemplary GPR test is shown in Fig. 1 (device during measurements and profile of the subsurface area).

The electro-resistance method is based on the analysis of the propagation of the generated electric current in the tested medium. This solution determines changes in the physical parameters of the tested object (resistivity).

Geoelectric imaging technologies can be divided as follows:

- Electrical Resistance Tomography (ERT)
- Induced Polarization Tomography (IPT)
- Self-Potential Tomography (SPT)
- Spectral Induced Polarization Tomography (SIP)
- Capacitive Resistivity Imaging (CRI)
- Automated time-Lapse Electrical Resistivity Tomography (ALERT)
- Complex Resistivity Tomography (CRT)

Electrical properties of objects vary depending on the substrate material as well as the presence and level of fluid saturation. The technique that reconstructs the image on the basis of electrical measurements is electrical resistance tomography (ERT). Voltage measurements on electors are made by introducing an electric current to the tested subsurface. Electro-resistance methods, including electro-resistance tomography, are particularly useful for studying the base of flood embankments. An example of the effective use of this method is the detection of organic sediments in the subsoil. An exemplary measurement of the ERT device and soil analysis has been shown in Fig. 2.

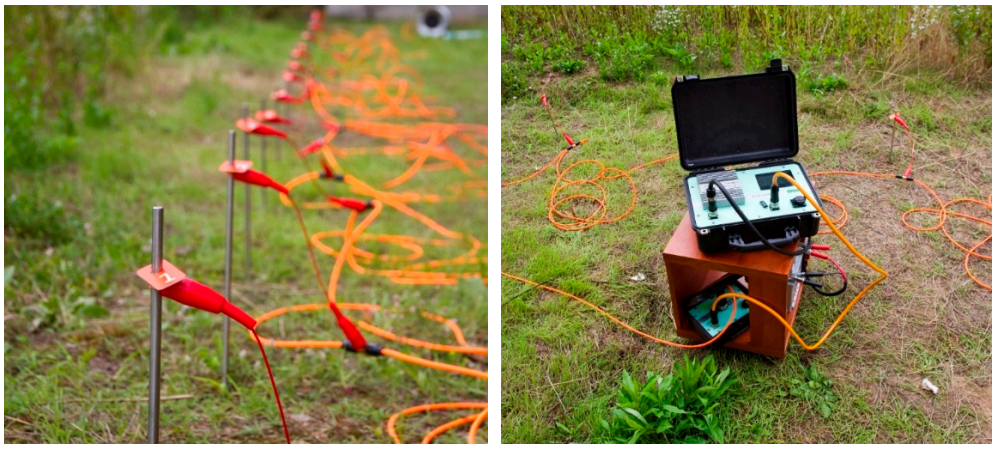

Figure 2. ERT measurement system: (a) an array of 32 ground electrodes, (b) device, (c) Typical resistivity imaging survey

Thermography is a technique, which is used to analyse various types of objects. It is one of the methods of thermal diagnostics using the phenomenon of non-contact detection of electromagnetic radiation in the mid-infrared band. During the measurement, the temperature distribution on the surface of the measured object is obtained. By analysing different thermal images taken at different times, some anomalies can be detected, such as leaks in flood embankments [12]. Figure 3 shows the

Preprints (www.preprints.org) | NOT PEER-REVIEWED | Posted: 20 August 2018 doi:10.20944/preprints201808.0346.v1

container with electrodes flooded with water and its infrared view.

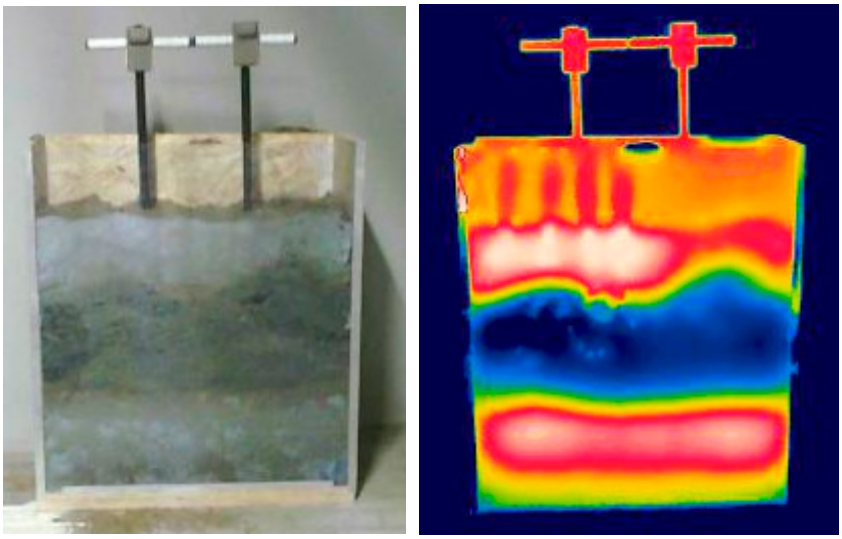

(a) (b)

Figure 3. Tank with electors flooded with water: (a) model view, (b) infrared view

The main purpose of this work is to present a system based on electrical impedance tomography, which enables monitoring flood embankments. The project was carried out as part of research at the Netrix Research and Development Laboratory. The solution concept is based on the construction of a distributed system for acquiring, processing and reconstructing measurement data from tomographic devices in a cloud computing system. This solution is particularly beneficial in the case of monitoring large and dispersed measuring objects. Our system has specially designed device for measuring tomography data, collecting and analysis this data by machine learning methods, making it an innovative solution for monitoring flood embankments.

The article has been divided into 5 chapters with the introduction. Chapter 2 presents the architecture of the designed system, devices and measuring sensors, analysed numerical models, laboratory measurements and the method of solving the inverse problem. Chapter 3 presents the results of image reconstruction for measurement models and selected reconstructions of real measurements. In Chapter 4, the results obtained are discussed, while in the 5th chapter, the performed research is summarized.

2. Materials and Methods

This chapter presents system architecture, numerical and laboratory models of flood embankments, measuring device and image reconstruction algorithms solving the inverse problem based on elastic net. Numerical models, simulation tests and analysis based on real measurements were prepared using the Eidors toolbox [13] and the R language code.

2.1 Architectire of system

The system architecture for monitoring flood embankments and the system consists of a set of measuring devices and applications placed in the cloud, as shown in Fig. 4. Data is collected from tomographic devices and transmitted to the analytical system. Data processing takes place in real time, data is collected in the database for additional offline analysis. The presented monitoring system is designed to identify changes in the construction of flood embankments with the use of electrical impedance tomography. The solution determines the humidity (damage) of the tested models. The monitoring system is based on a distributed structure for the acquisition, processing and analysis of measurement data. The key element of the solution is measuring devices for collecting and sending data to the Cloud Computing module and algorithms for their further analysis (Fig. 5). The hardware solution consists of mobile units equipped with wireless data transfer using Message Queuing

Preprints (www.preprints.org) | NOT PEER-REVIEWED | Posted: 20 August 2018 doi:10.20944/preprints201808.0346.v1

Telemetry Transport (MQTT). The system has a specially designed measuring structure. The monitoring system consists of 5 layers (Fig. 6): measurement sensors, data transmission, data collection, data analysis and user interface. The sensor layer is a source of data from measuring devices, subjected to further analysis. The data is then sent via the MQTT protocol to the hub, whose task is to integrate the measurement section and send them to the MQTT broker. The data transmission layer integrates the sensor layers with the analytical layer, which includes a data collection module. In the case of real-time data analysis, the analytical value is used. Storage is intended to collect data received from the analytical system. Current and historical data form the basis for further analyses [14-18].

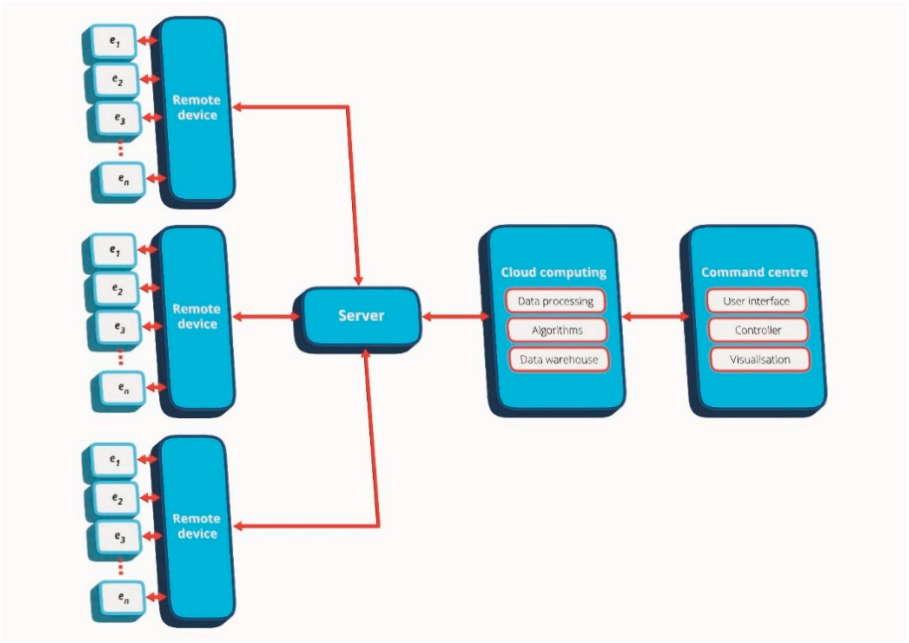

Figure 4. Model of a multi-sensor distributed system based on the Internet of Things and CPS

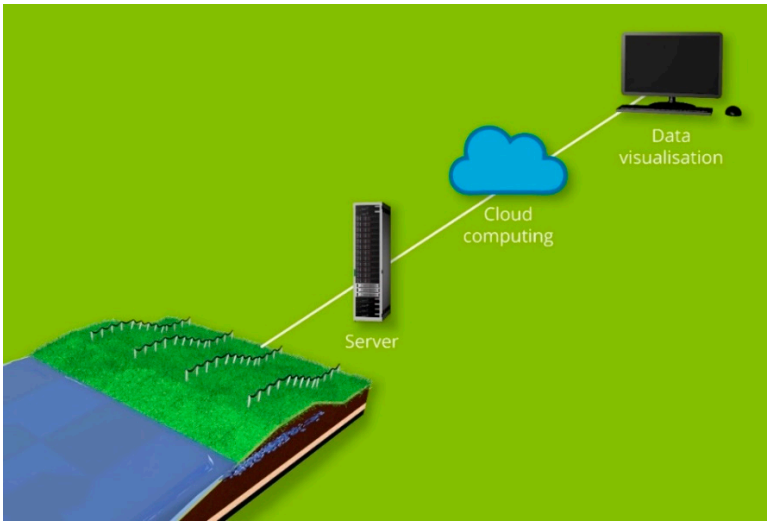

Figure 5. The system model for monitoring flood embankments

Preprints (www.preprints.org) | NOT PEER-REVIEWED | Posted: 20 August 2018 doi:10.20944/preprints201808.0346.v1

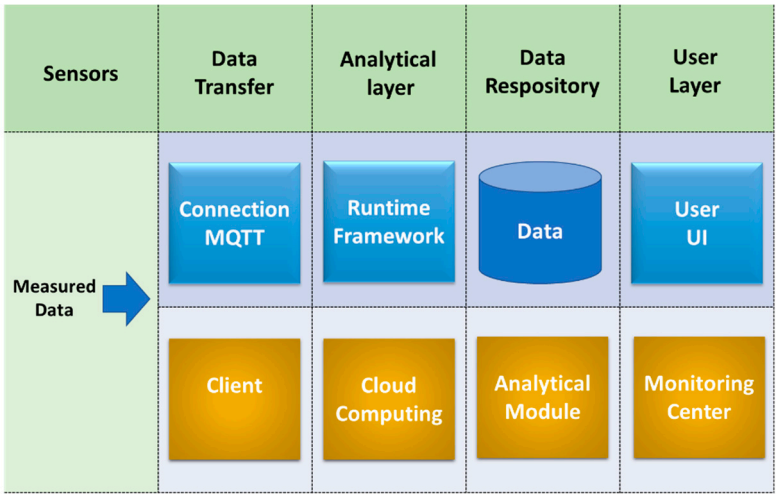

Figure 6. Schematic diagram of the data collection and analysis system

2.2 Electrical impedance tomography

Electrical impedance tomography (EIT) [19,20] sometimes referred to more generally as electrical tomography (ET) [21-26] involves several techniques for image reconstruction. The literature includes the following methods: electrical capacitance tomography (ECT) [27-30], electrical resistive tomography (ERT) [31] and electrical impedance tomography [32,33]. Electrical capacitance tomography is based on the reconstruction of the electrical permittivity ε [34-36], while the electrical impedance tomography reconstructs the conductivity γ [37-39]. In the case of resistive character of the tested environment, the electrical resistance tomography (ERT) [40,41] is also used, which is based on electrical measurements similar to EIT.

In the EIT, the voltage or current is injected into the object with a set of electrodes attached to its surface. The voltage values are measured on the remaining electrodes. The conductivity of the object is reconstructed based on the measurements made and an appropriate algorithm to solve the inverse problem. Forward problem is described by the Laplace equation:

$$\nabla\cdot(\gamma\nabla u)=0, \tag{1}$$

where: u is electrical potential and γ is conductivity.

2.3 Measurements system

The device based on electrical impedance tomography measures the tested object based on measurements of the potential distribution on the surface. The system collects the measured data from the electrodes. The presented device for electrical tomography assumes the use of two measurement methods and allows measurements to be made up to 32 channels. The device consists of several separate modules: a current generator, a measuring block, a multiplexer and a controller. More than one multiplexer can be connected to the system. Data acquisition systems require equipment to measure voltage, filter, demodulate and convert to digital and signal processing units to transfer data to a computer. Depending on the method of use, the solution may be located in a large area or it may be enclosed in a small housing. In both cases, the entire infrastructure is centrally managed to collect data and record measurements. The application allows to collect measurements, manage data and monitor devices. The electric tomograph is shown in Fig. 7.

Preprints (www.preprints.org) | NOT PEER-REVIEWED | Posted: 20 August 2018 doi:10.20944/preprints201808.0346.v1

Figure 7. An electrical tomograph for measurements in electrical tomography

2.4 Measurement models

Electrical impedance tomography provides a non-invasive technique for measuring various types of objects. The following are 7 measurement models with two types of electrodes, by means of which measurements of the internal properties of objects can be analysed by means of measurements on the edge or near the surface of the examined area. The data collection system collects the measured voltage from the electrodes and then processes them. Figures 8 and 9 show a model of measuring systems based on 16 and 32 electrodes. Figures 10 and 11 illustrate the measurement models where multi-sensor electrodes were used.

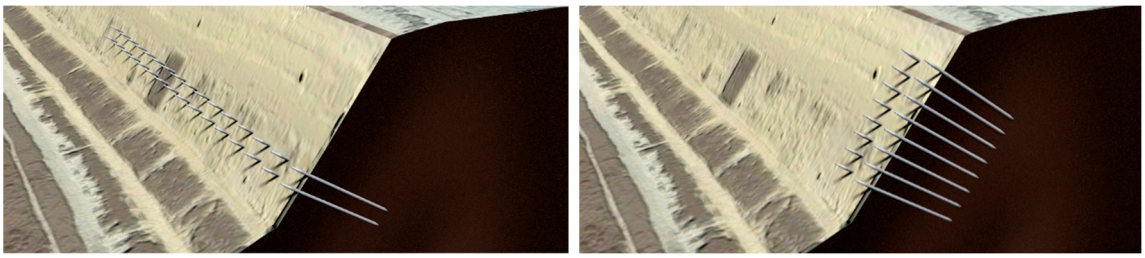

(a) (b)

Figure 8. Model of flood embankment with uniform measuring electrodes: (a) measurement along the tested object, (b) measurement across the tested object

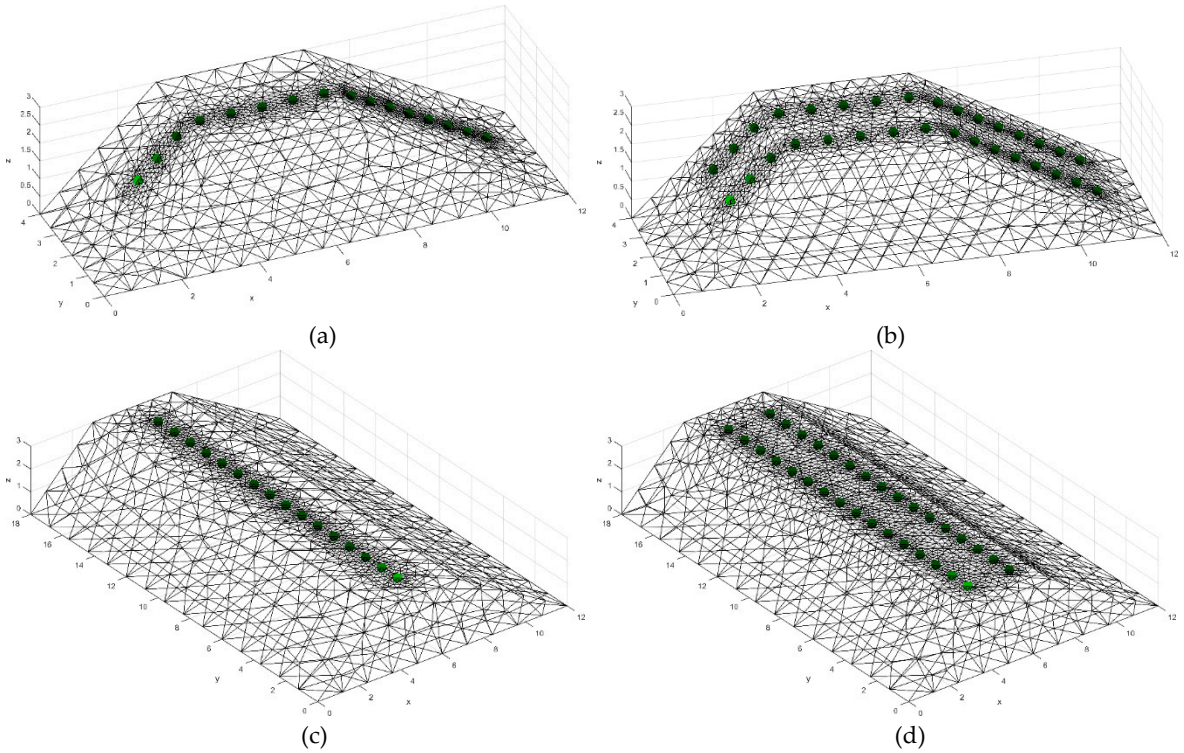

(a) (b)

(c) (d)

Preprints (www.preprints.org) | NOT PEER-REVIEWED | Posted: 20 August 2018 doi:10.20944/preprints201808.0346.v1

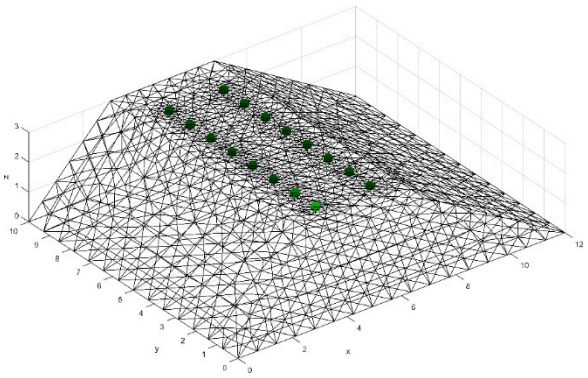

(e)

Figure 9. Numerical models of flood embankments: (a) Model I with 16 measuring electrodes, (b) Model II with 32 measuring electrodes, (c) Model III with 16 measuring electrodes, (d) Model IV with 32 measuring electrodes, (e) Model V with 16 measuring electrodes

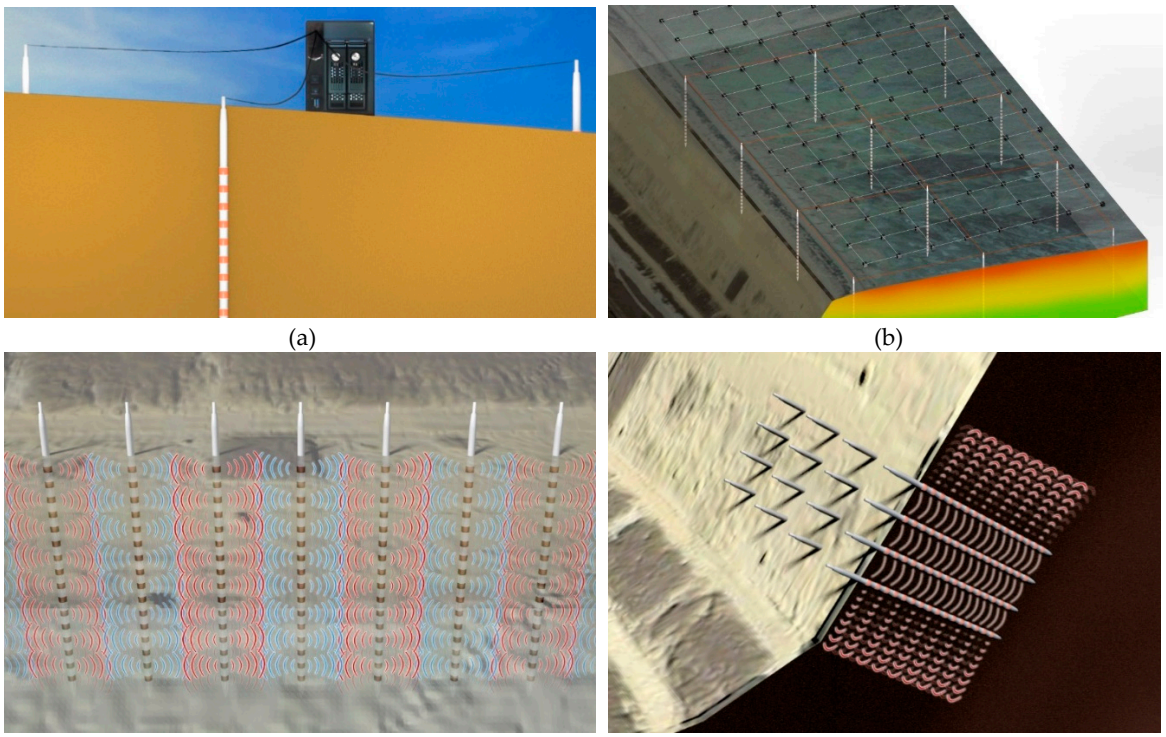

(a) (b)

(c) (d)

Figure 10. Model of flood embankment with multi-sensor electrodes: (a) the measurement model, (b) the area distribution of sensors, (c) the view in the longitudinal section, (d) the cross-sectional view

Preprints (www.preprints.org) | NOT PEER-REVIEWED | Posted: 20 August 2018 doi:10.20944/preprints201808.0346.v1

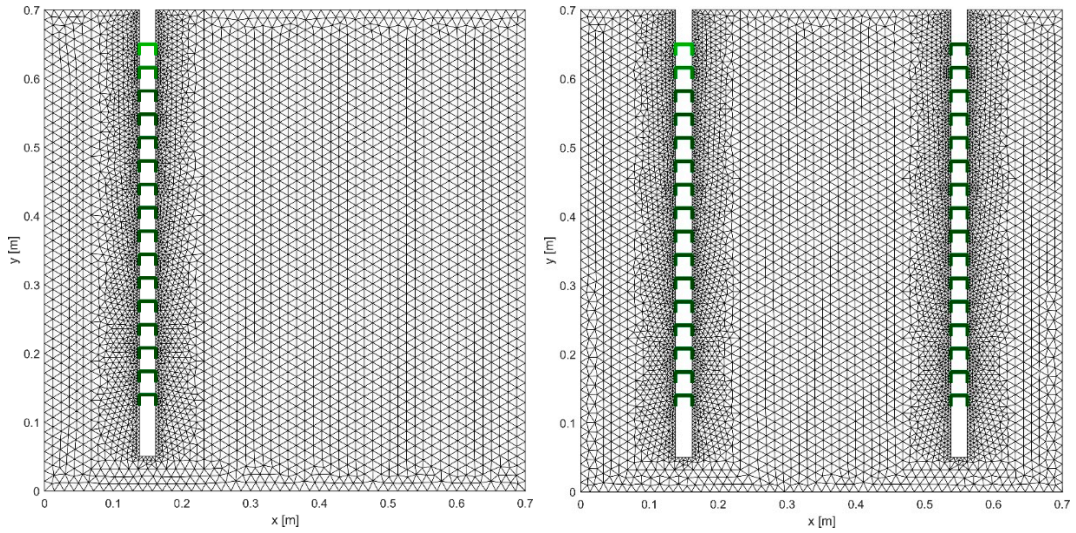

(a) (b)

Figure 11. Numerical models of multi-sensor electrodes (a) Model VI with 16 measurement points, (b) Model VII with 32 measurement points

2.5 Laboratory models

In the presented laboratory stands, the set of electrodes was placed in the body of the object models. Measurements were made for the presented sets. Figure 12 shows a laboratory system with 32 measuring electrodes in the form of the model itself as well as during the measurement with an electrical tomograph. Figures 13 and 14 show laboratory measurement models with one and two multi-sensor electrodes.

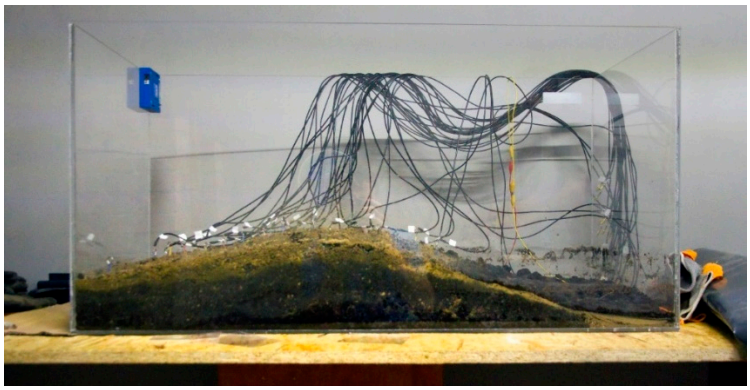

(a)

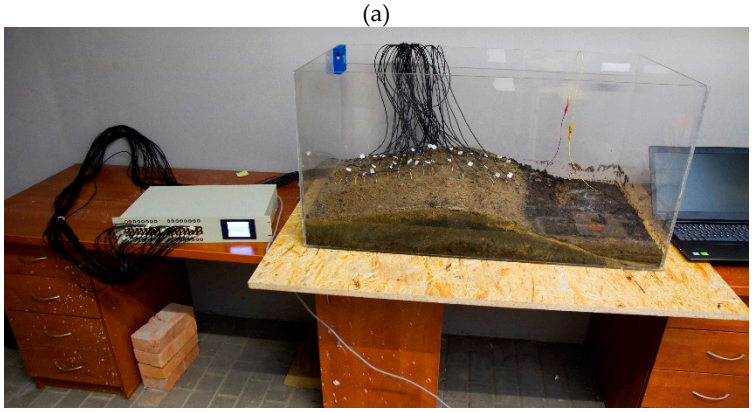

(b)

Figure 12. Laboratory system with 32 measuring electrodes: (a) model of flood embankment, (b) model during measurements with an electrical tomograph

Preprints (www.preprints.org) | NOT PEER-REVIEWED | Posted: 20 August 2018 doi:10.20944/preprints201808.0346.v1

(a) (b)

Figure 13. Laboratory model with one multi-sensor electrode: (a) front view, (b) top view

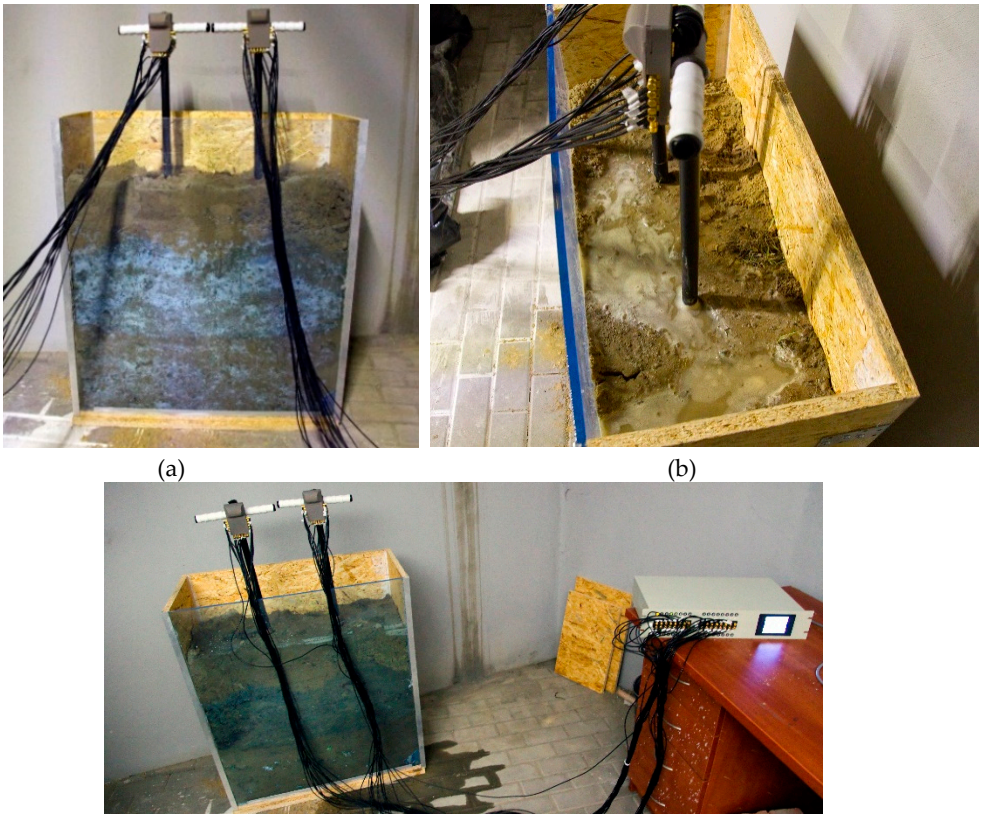

(a) (b)

(c)

Figure 14. Laboratory model with one multi-sensor electrode: (a) front view, (b) top view, (c) during electrical tomography measurements

2.6. Machine Learning

There are many optimization methods [42-53]. In this article, the authors focused on the application of machine learning algorithms. There methods rely on algorithms that use information to learn directly from data without first specifying a mathematically defined model. Applied artificial intelligence algorithms and machine learning use the availability of large amounts of data and computational resources, which is their characteristic feature at present. The main idea of these methods is to prepare a model from a finite training set, which generalizes the characteristic properties of the problem under investigation. Such a model reflects the real problem on the basis of prepared and trained examples, cannot at the same time introduce too close dependence on the training set itself. Statistical inference involves building a probabilistic model based on a certain type

Preprints (www.preprints.org) | NOT PEER-REVIEWED | Posted: 20 August 2018 doi:10.20944/preprints201808.0346.v1

of knowledge a priori. Often the amount of information available is very large due to the number of functions that characterize a given problem [54].

2.7. Identification of linear models

The data being analysed is often highly correlated and there is a need to select important groups of variables. The least squares method is used to estimate parameters, which minimizes the residual sum of squares. However, in the case of multidimensional data, this method is not good at predicting the accuracy and interpretation of the model. In multidimensional problems, predictors are usually strongly correlated. A good model needs to be built to achieve the desired effect by looking for a solution in high-parameter data analysis. Here, the elastic net method was presented, which causes rare solutions, encouraging group selection, where strongly correlated predicators are usually chosen or rejected together. Ridge and LASSO regularization helps in the selection of a possible solution. Elastic net is a linear combination of L_1 and L_2 penalties. This method combines the useful properties of ridge and LASSO regularization [55].

Multicollinearity in statistics is a phenomenon in which two or more predictor variables in a multiple regression model are strongly correlated. Backbone regression is a common way to solve a multicollinearity problem where there is no unique solution for the least squares method.

We are considering a linear regression model, where X is the predictor matrix and the ridge coefficients are defined as

$$\hat{\beta}^{ridge} = \arg\min_{\beta \epsilon R^k} \|Y - X\beta\|_{L_2} + \lambda\|\beta\|_{L_2}, \quad (2)$$

where $\|\beta\|_{L_2} = \|\beta\|^2 = \langle\cdot,\cdot\rangle$ is a scalar product, the tuning parameter λ has a positive value (λ>0).

Equation (2) has a unique solution. When it ranges from 0 to 1, it balances the two options: adjusting the linear y and X model and reducing the coefficients. Ridge regression allows you to reduce the coefficients to zero by imposing a L_2 penalty. It cannot accurately reset zero. It allows assign close coefficients to highly correlated variables, but it cannot perform a variable selection (for specific real coefficients that are exactly zero).

LASSO is characterized by several advantages combining ridge with a variable selection. We are considering a linear regression model where LASSO estimates are defined as

$$\hat{\beta}^{lasso} = \arg\min_{\beta \epsilon R^k} \|Y - X\beta\|_{L_2} + \lambda\|\beta\|_{L_1}, \quad (3)$$

where $\|\beta\|_{L_1} = \frac{1}{k}\sum_{i=1}^{k}|\beta_i|$ and λ>0.

LASSO causes some coefficients to be shortened to zero exactly because of the L_1-penalty geometry. This method can select variables, which is essentially different from ridge regression. LASSO, however, has some limitations, it tends to choose only one variable from the group and it is not for this method which one is chosen.

Simulation research and real data show that elastic net often exceeds LASSO, encourages grouping effect, where strongly correlated predictors occur together in a given model or outside of it. The method is particularly useful when the number of predictors is much larger than the number of observations [56].

The problem of identification of linear dependencies is well known in the literature of the subject. Let us consider the problem of identification of dependence, which is described by the linear equation

$$Y = X\beta + \varepsilon, \quad (4)$$

where $Y \in R^n, X \in R^{n\times(k+1)}$ are the observation matrices of a dependent variable and independent variables respectively, $\beta \in R^{k+1}$ denotes the matrix of unknown structural parameters. In the state equation (4) the vector $\varepsilon \in R^n$ represents the external disturbances. We assume additionally, that the sequence $\{\varepsilon_t\}_{1\le t\le n}$ is a sequence of independent identically distributed random variables with normal distribution $N(0, \sigma^2)$. The classical least square method consists in determining the unknown parameters $\beta = (\beta_0, \beta_1, \dots, \beta_k)$. In the equation (4) by solution the task

Preprints (www.preprints.org) | NOT PEER-REVIEWED | Posted: 20 August 2018 doi:10.20944/preprints201808.0346.v1

$$\min_{\beta \in R^{k+1}} \|Y - X\beta\|^2. \tag{5}$$

If $\det(X^T X) \neq 0$, then from Gauss-Markov Theorem we obtain, that the best linear unbiased estimator of unknown parameters β is equal $\hat{\beta} = (X^T X)^{-1} XY$.

In a case when the number of independent variables in the equation (4) is quite large, then the problem arises to select these variables to the model. Among the family of models (this family includes 2^k models) one should choose the model that best characterizes this dependence. Usually the procedure for selecting the "best" model consists in adding or removing variables (forward selection, backward elimination) or a combination of these methods. In the literature it is called stepwise regression. This procedure is a time-consuming. An additional problem that occurs during the identification of dependences in equation (4) is the collinearity of independent variables. Undoubtedly, this is a big problem in tomography, because the measurements between some electrodes are strongly correlated. If the independent variables are strongly correlated (collinear), then the matrix $X^T X$ tends to singular matrix.

Directly using the least square method we get a large mean square error of estimators of unknown parameters (sum of variance and square bias of estimator) $MSE(\hat{\beta}) = \mathrm{var}(\hat{\beta}) + bias^2(\hat{\beta})$.

The predictions obtained from models with a large mean square error of estimators are quite unstable. The one of possible solution of this problem consist in adding an additional penalty to the objective function in the task (5), where the value of penalty depends on the values of parameter estimators. Imposing a penalty on large values of parameters causes that the estimators are pulled towards to zero (it is causing that the estimators are shrinking). The effect of such action is the reduction of the variance of estimators, and in consequence the quality of prediction of model is improved. Unfortunately, the received estimators are biased.

Below, we will describe the elastic net method proposed by [56]. This method is a combination of ridge regression (called Tikhonov regularization, is one of the oldest methods of model regularization) and Least Absolute Shrinkage and Selection Operator (LASSO). The penalty function is described as linear combination L_1 and L_2 norms of unknown parameters in model (4). From above the penalty is defined as

$$P_\alpha(\beta') = (1-\alpha)\frac{1}{2}\|\beta'\|_{L_2} + \alpha\|\beta'\|_{L_1} = \sum_{j=1}^{k}\left(\frac{1-\alpha}{2}\beta_j^2 + \alpha|\beta_j|\right), \tag{6}$$

where $\beta = (\beta_0, \beta')$ and $\beta' = (\beta_1, \ldots, \beta_k)$, whereas $0 \leq \alpha \leq 1$. The unknown parameters in model (4) we determine by solution the task

$$\min_{(\beta_0, \beta') \in R^{k+1}} \frac{1}{2n}\sum_{i=1}^{n}(y_i - \beta_0 - x_i\beta')^2 + \lambda P_\alpha(\beta'), \tag{7}$$

where $x_i = (x_{i1}, \ldots, x_{ik})$ for $1 \leq i \leq n$, whereas the parameter $\lambda > 0$ defines the penalty coefficient. In formula (6) the parameter $0 \leq \alpha \leq 1$ creates the creates the compromise between LASSO ($\alpha = 1$) and ridge regression ($\alpha = 0$). For ridge regression the penalty is calculated in L_2 norm, whereas for LASSO in L_1 norm. Elastic net is a joint of ridge regression and LASSO. As a result of the LASSO method, we obtain sparse models, where part of estimators of unknown parameters is equal zero. Regression LASSO was proposed by [57] and it consists in the estimation of unknown parameters and the choice the variables to model. The application of ridge regression causes that part of coefficients shrinkages (tends to zero), but it does not eliminate the variables in model. The estimators obtained from ridge regression, LASSO or elastic net are biased estimators. By introducing the bias to estimators, we expect the improving of quality of prediction. The estimation time is also much smaller than in the case when we use stepwise regression.

For different values λ and α we obtain different estimators $\hat{\beta}(\alpha, \lambda)$ of unknown parameters β in linear model (4). The values α and λ we determini by minimizing the mean square terror of prediction $F(\alpha, \lambda) = \left\|Y - X\hat{\beta}(\alpha, \lambda)\right\|^2$ for $0 \leq \alpha \leq 1, \lambda > 0$. In image reconstruction the values of finite elements we determine by using the equation

$$\hat{Y} = X\hat{\beta}(\alpha, \lambda), \tag{8}$$

Preprints (www.preprints.org) | NOT PEER-REVIEWED | Posted: 20 August 2018 doi:10.20944/preprints201808.0346.v1

where $\hat{\beta}(\alpha,\lambda) = (\hat{\beta}_0, \hat{\beta}_1, \ldots, \hat{\beta}_k)$ is an estimator of unknown parameters obtained using the elastic net method [58-61].

2.8. Example of image reconstruction by elastic net

In order to verify the effectiveness of the proposed method in the previous chapter, an example based on EIT in the form of a rectangular object with 16 measurement points was implemented. Image Reconstruction reflect the image 64 * 32 = 2048 (for each pixel creates a linear model with 208 correlated predictors: 16 projection angles times 13 volts). Figure 15 shows an example of image reconstruction with different types of four interposed objects. The image has been reconstructed with high precision.

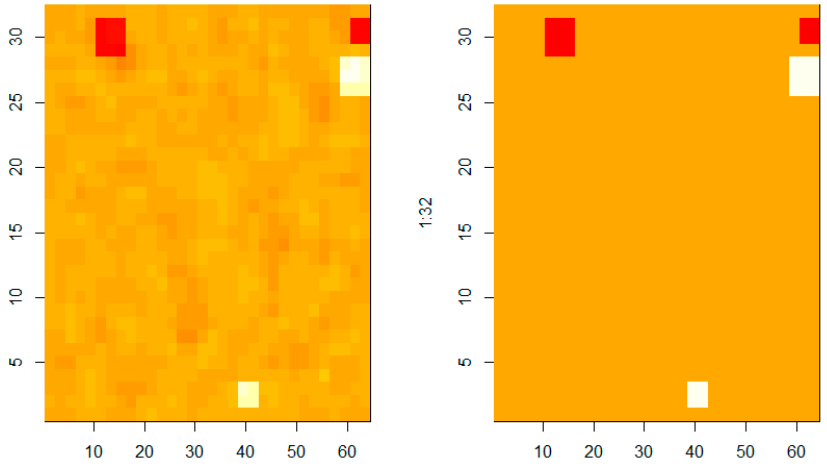

Figure 15. Example of image reconstruction for 4 unknown objects using the elastic net method: (a) result, (b) pattern

2.9. Methods of stimulating research objects

In the Eidors package, the method of stimulation of the tested object is defined by three components. For each projection angle:

- indicate the current electrodes,
- determine the current flowing through the object,
- determine the sequence of measuring electrical voltages.

Table 1. Measurement method I

		1		2		3	
Current		1	4	2	5	3	6
Voltage	1	2	3	3	4	1	2
	2	5	6	6	7	4	5
	3	6	7	7	8	7	8
	4	7	8	8	9	8	9
	5	8	9	9	10	9	10
	6	9	10	10	11	10	11
	7	10	11	11	12	11	12
	8	11	12	12	13	12	13
	9	12	13	13	14	13	14
	10	13	14	14	15	14	15
	11	14	15	15	16	15	16
	12	15	16	16	1	16	1

Preprints (www.preprints.org) | NOT PEER-REVIEWED | Posted: 20 August 2018 doi:10.20944/preprints201808.0346.v1

The first method of stimulation covers as many projection angles as there are electrodes connected to the tested object (Table 1). In the j -th projection angle, the electrodes assigned the numbers j and $j \oplus 3$ are the current electrodes. The voltages were measured between two adjacent electrodes - excluding the current electrodes. As a result, a single cycle includes $N \cdot (N-4)$ voltage measurements, where N is the number of all electrodes. Thus, for $N = 16$ we have 192 measurements, while for $N = 32$ we have 896 measurements. The table below presents a list of ordered pairs of current and voltage electrodes for the first three projection angles at $N = 16$.

In the second method of stimulation, the number of projection angles equals half the number of electrodes connected to the tested object (Table 2). In the j-th projection angle, electrodes with the numbers j and $j+\frac{1}{2}N$ are current electrodes. As in the previous stimulation, voltage measurements take place between two adjacent electrodes, obviously omitting the current electrodes. As a result, a single cycle includes $\frac{1}{2}N \cdot (N-4)$ voltage measurements. In this case, for $N = 16$ we have 96 measurements, while for $N = 32$ we have 448 measurements. The table below presents a list of ordered pairs of current and voltage electrodes for the first three projection angles at $N = 16$.

Table 2. Measurement method II

		1		2		3	
Current		1	9	2	10	3	11
Voltage	1	2	3	3	4	1	2
	2	3	4	4	5	4	5
	3	4	5	5	6	5	6
	4	5	6	6	7	6	7
	5	6	7	7	8	7	8
	6	7	8	8	9	8	9
	7	10	11	11	12	9	10
	8	11	12	12	13	12	13
	9	12	13	13	14	13	14
	10	13	14	14	15	14	15
	11	14	15	15	16	15	16
	12	15	16	16	1	16	1

3. Results

This chapter presents the results of water leaks in flood embankments on the basis of built numerical models and laboratory measurements. The forward problem was solved by the finite element method. The inverse problem was solved by the elastic net method with ridge and LASSO regularization.

3.1. Image reconfiguration results for Model I

The three-dimensional model I represents a fragment of a flood embankment. All electrodes are on one surface, which is perpendicular to the riverbed. This means that in this case the electrodes are arranged across the shaft.

Model parameters:

- number of nodes: 2346,
- number of tetrahedrons: 9853,
- number of electrodes: 16,
- type of electrodes: points.

For two methods of stimulation (stimulation 1 contains 192 measurements, stimulation 2 contains 96 measurements) the parameters of linear models were estimated using elastic net. The parameter $\lambda = 7 \cdot 10^{-6}$ and $\alpha = 0.8$ was assumed. The reconstruction results are shown in Fig. 16-18.

Experimental conclusions:

Preprints (www.preprints.org) | NOT PEER-REVIEWED | Posted: 20 August 2018 doi:10.20944/preprints201808.0346.v1

- The use of stimulation 1 (increase in the number of measurements) visually did not improve the quality of reconstruction in relation to the reconstruction using stimulation 2.
- Poor reconstruction in case of side seepage of the shaft or a small central one.
- With the model I it is quite good to reconstruct the depth of seepage of the embankment and the length of seepage.

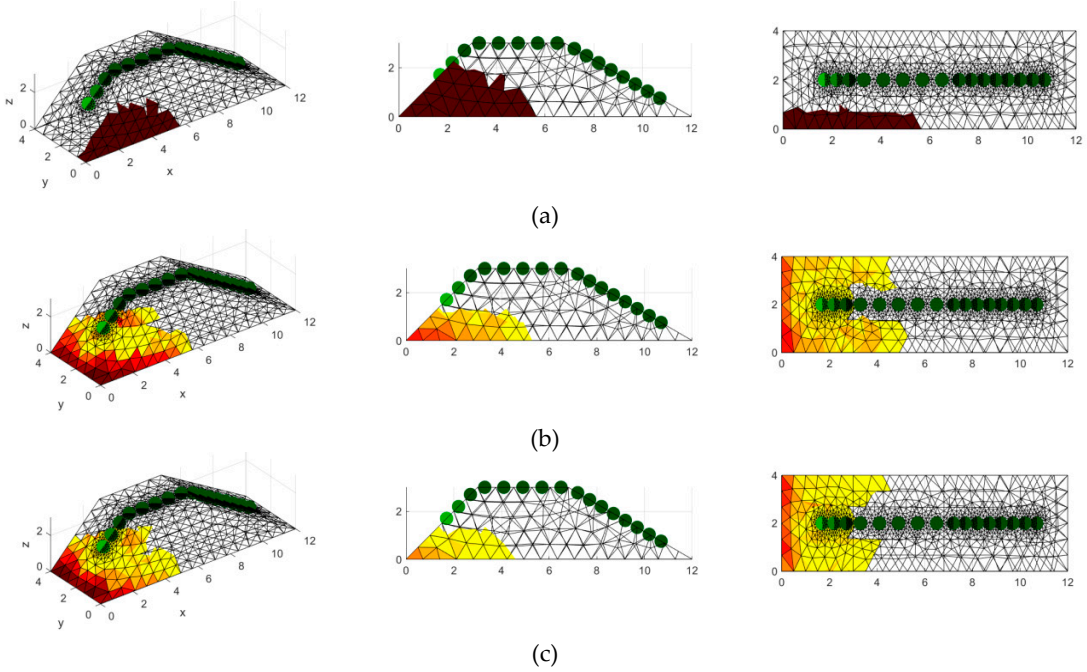

Figure 16. Model I flood embankment with 16 electrodes – side infiltration of water: (a) pattern, (b) simulation 1, (c) simulation 2

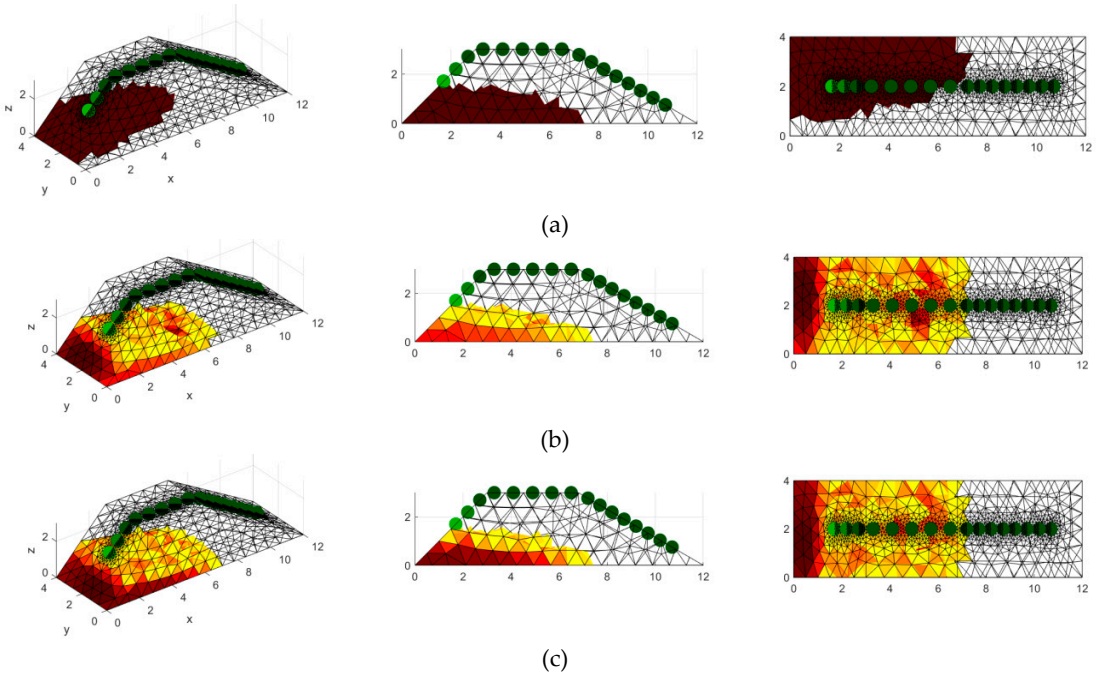

Figure 17. Model I flood embankment with 16 electrodes – side-central infiltration of water: (a) pattern, (b) simulation 1, (c) simulation 2

Preprints (www.preprints.org) | NOT PEER-REVIEWED | Posted: 20 August 2018 doi:10.20944/preprints201808.0346.v1

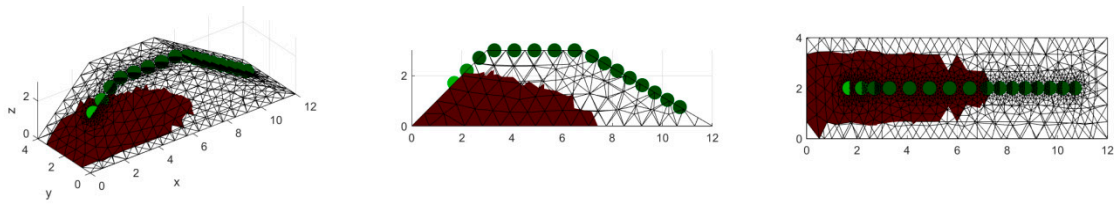

(a)

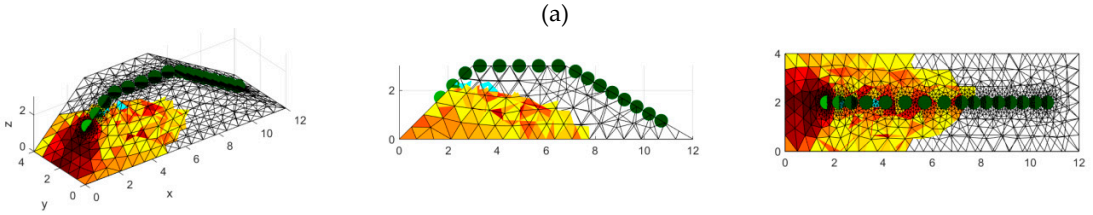

(b)

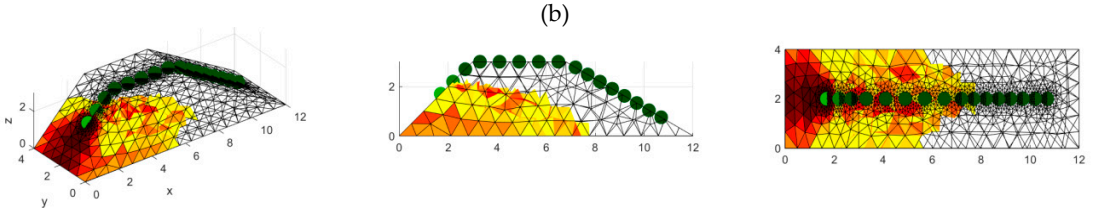

(c)

Figure 18. Model I flood embankment with 16 electrodes – central narrow infiltration of water: (a) pattern, (b) simulation 1, (c) simulation 2

3.2. Image reconfiguration results for Model II

The three-dimensional model II represents a fragment of a flood embankment. All electrodes are in two planes, which are perpendicular to the riverbed. This means that in this case the electrodes are arranged perpendicular to the shaft.

Model parameters:

- number of nodes: 2991,
- number of tetrahedrons: 12,153,
- number of electrodes: 32,
- type of electrodes: points.

For two methods of stimulation (stimulation 1 contains 896 measurements, stimulation 2 contains 448 measurements) the parameters of linear models were estimated using elastic net. The reconstruction results are shown in Fig. 19-21.

Experimental conclusions:

- Increasing the number of measurements visually did not improve the quality of reconstruction.
- Placing the electrodes in two planes (in comparison to the I model) perpendicularly to the river bed significantly improved the reconstruction during lateral seepage of the embankment.
- With the help of Model II, it is quite good to reconstruct the depth of seepage of the embankment and the length of the seepage.

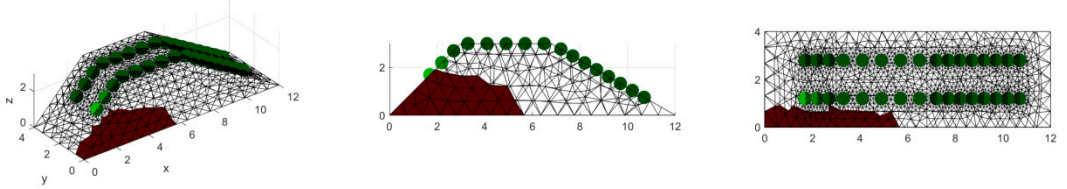

Preprints (www.preprints.org) | NOT PEER-REVIEWED | Posted: 20 August 2018 doi:10.20944/preprints201808.0346.v1

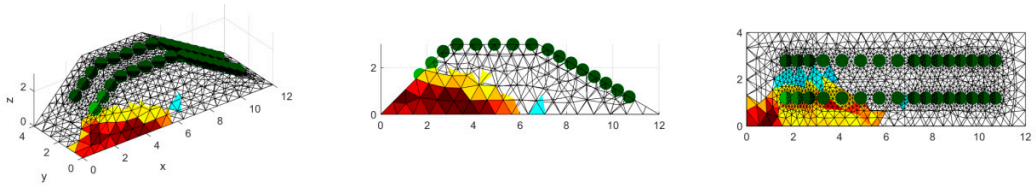

(a)

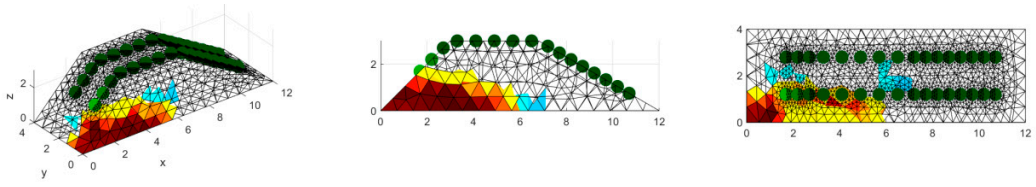

(b)

(c)

Figure 19. Model II flood embankment with 32 electrodes – side infiltration of water: (a) pattern, (b) image reconstruction 1, (c) image reconstruction 2

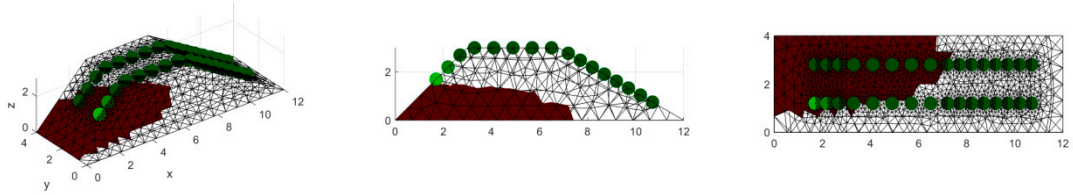

(a)

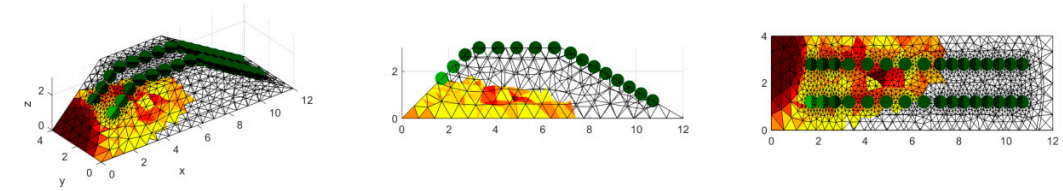

(b)

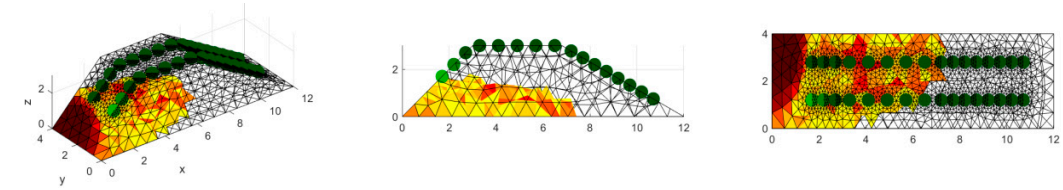

(c)

Figure 20. Model II flood embankment with 32 electrodes – back-side infiltration of water: (a) pattern, (b) image reconstruction 1, (c) image reconstruction 2

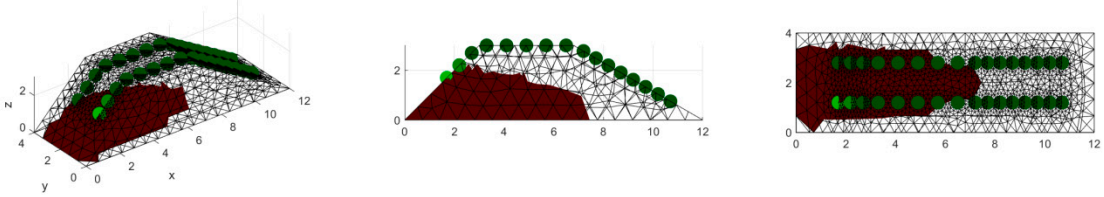

(a)

Preprints (www.preprints.org) | NOT PEER-REVIEWED | Posted: 20 August 2018 doi:10.20944/preprints201808.0346.v1

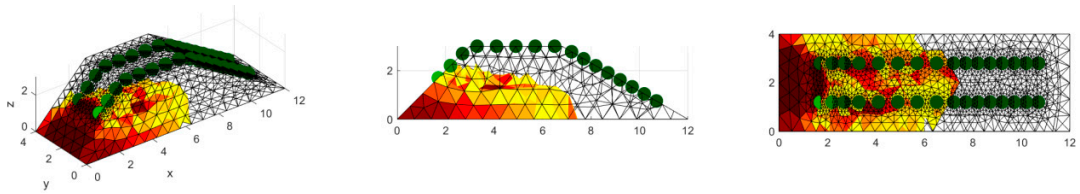

(b)

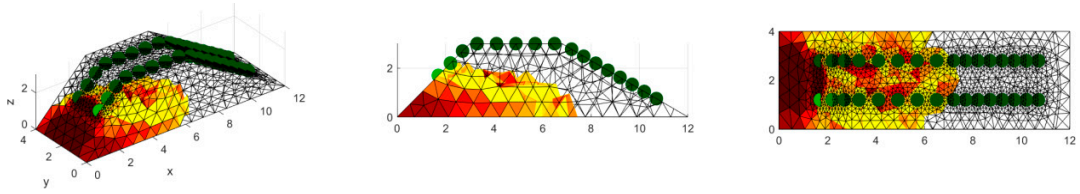

(c)

Figure 21. Model II flood embankment with 32 electrodes – central infiltration of water: (a) pattern, (b) image reconstruction 1, (c) image reconstruction 2

3.3. Image reconfiguration results for Model III

The three-dimensional model III represents a fragment of the flood embankment. All electrodes are in one plane, which is parallel to the river bed. This means that in this case the electrodes are arranged along the shaft.

Model parameters:

- number of nodes: 2231,
- number of tetrahedrons: 9341,
- number of electrodes: 16,
- type of electrodes: points.

For two methods of stimulation (stimulation 1 contains 192 measurements, stimulation 2 contains 96 measurements) the parameters of linear models were estimated using elastic net. The reconstruction results are shown in Fig. 22-24.

Experimental conclusions:

- Increasing the number of measurements visually improved the quality of the reconstruction at initial permeation.
- Placing the electrodes in one plane parallel to the river bed poorly reconstructs initial seepage.
- With the help of Model III, it is quite good to reconstruct the depth of seepage of the embankment and the length of seepage.

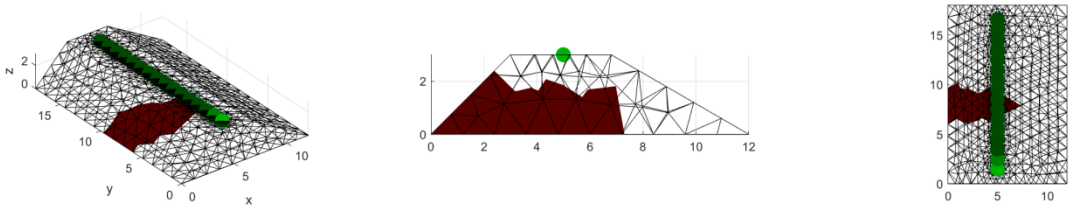

(a)

Preprints (www.preprints.org) | NOT PEER-REVIEWED | Posted: 20 August 2018 doi:10.20944/preprints201808.0346.v1

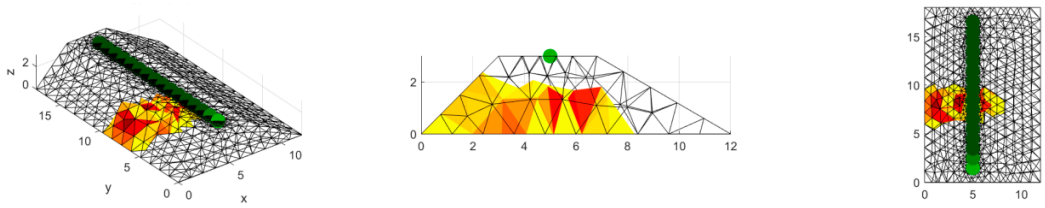

(b)

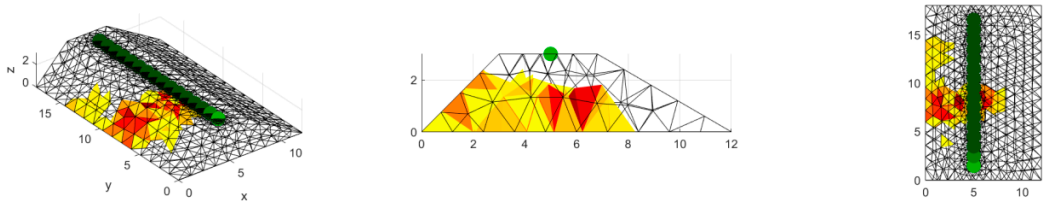

(c)

Figure 22. Model III flood embankment with 16 electrodes – central infiltration of water: (a) pattern, (b) image reconstruction 1, (c) image reconstruction 2

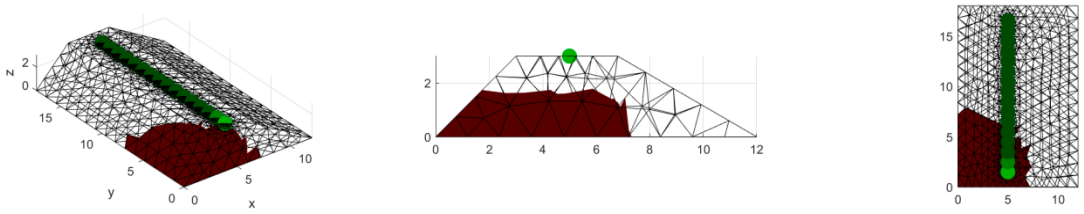

(a)

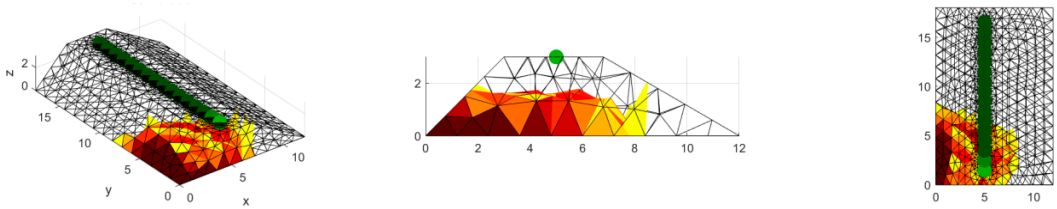

(b)

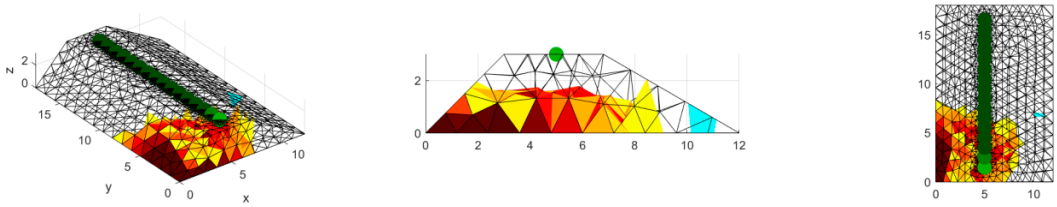

(c)

Figure 23. Model III flood embankment with 16 electrodes – side infiltration of water: (a) pattern, (b) image reconstruction 1, (c) image reconstruction 2

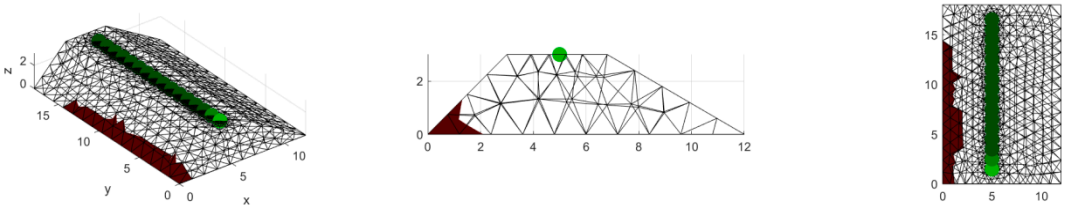

(a)

Preprints (www.preprints.org) | NOT PEER-REVIEWED | Posted: 20 August 2018 doi:10.20944/preprints201808.0346.v1

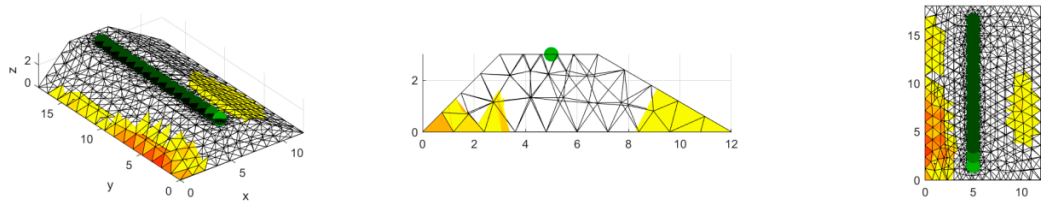

(b)

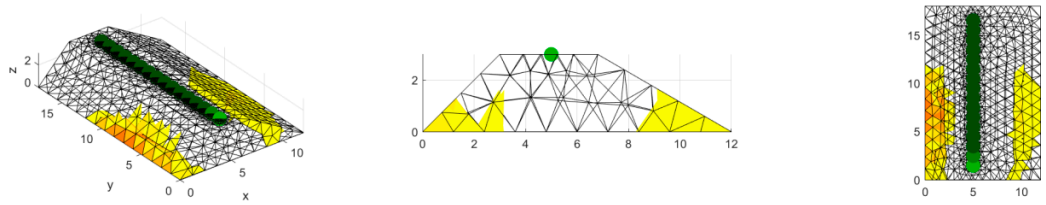

(c)

Figure 24. Model III flood embankment with 16 electrodes – small central infiltration of water: (a) pattern, (b) image reconstruction 1, (c) image reconstruction 2

3.4. Image reconfiguration results for Model IV

The three-dimensional IV model represents a fragment of the flood embankment. All electrodes are in two planes, which are parallel to the riverbed. This means that in this case the electrodes are arranged along the shaft.

Model parameters:

- number of nodes: 4002,
- number of tetrahedrons: 17191,
- number of electrodes: 32,
- type of electrodes: points.

For two methods of stimulation (stimulation 1 contains 896 measurements, stimulation 2 contains 448 measurements) the parameters of linear models were estimated using elastic net. The reconstruction results are shown in Fig. 25-27.

Experimental conclusions:

- Increasing the number of measurements visually did not improve the quality of reconstruction.
- Placement of electrodes in two planes parallel to the river bed significantly improved the reconstruction during lateral seepage of the embankment. Well recognizes infiltration at the beginning (small along the riverbed)
- With the IV model it is quite good to reconstruct the depth of seepage of the embankment and the length of seepage.

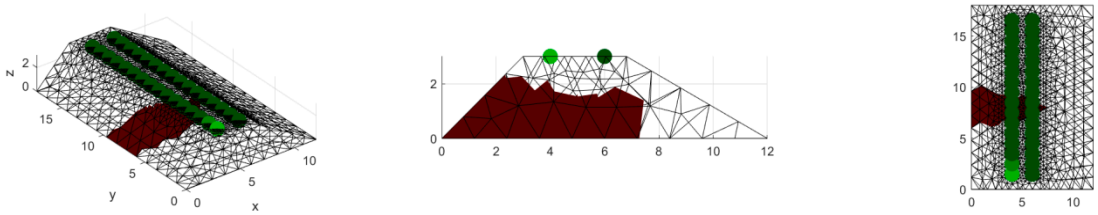

(a)

Preprints (www.preprints.org) | NOT PEER-REVIEWED | Posted: 20 August 2018 doi:10.20944/preprints201808.0346.v1

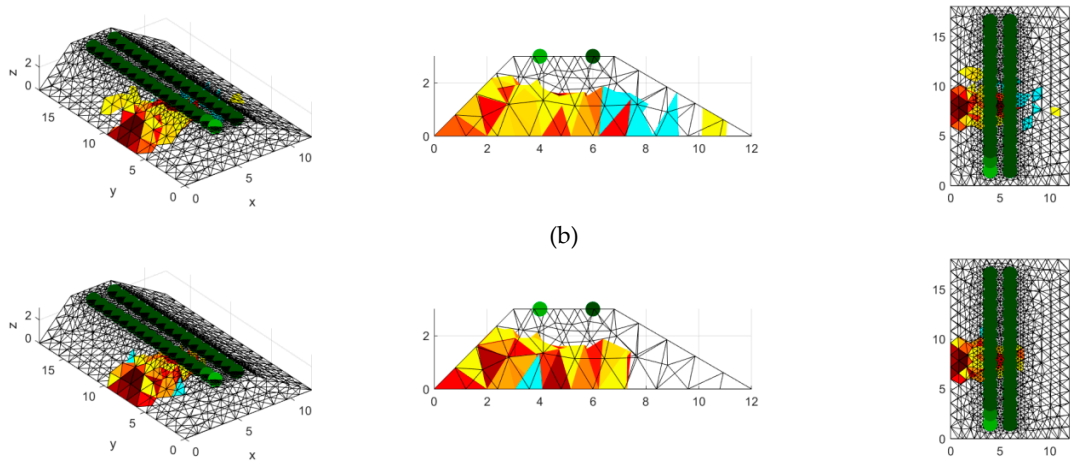

(b)

(c)

Figure 25. Model IV flood embankment with 32 electrodes – central infiltration of water: (a) pattern, (b) image reconstruction 1, (c) image reconstruction 2

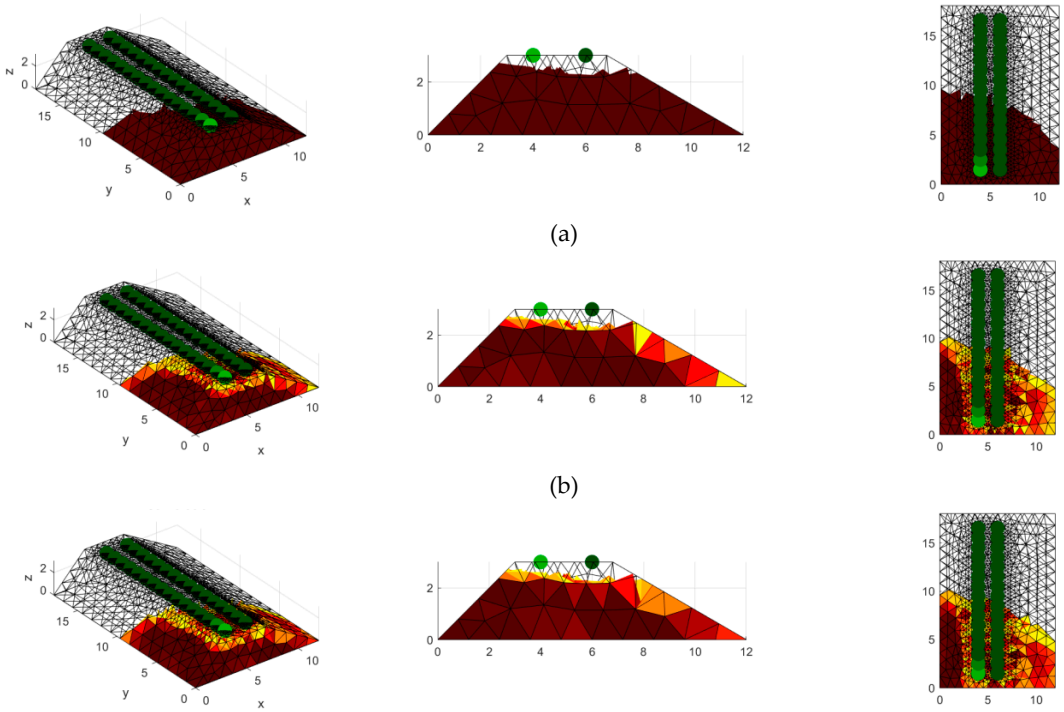

(a)

(b)

(c)

Figure 26. Model IV flood embankment with 32 electrodes – side infiltration of water: (a) pattern, (b) image reconstruction 1, (c) image reconstruction 2

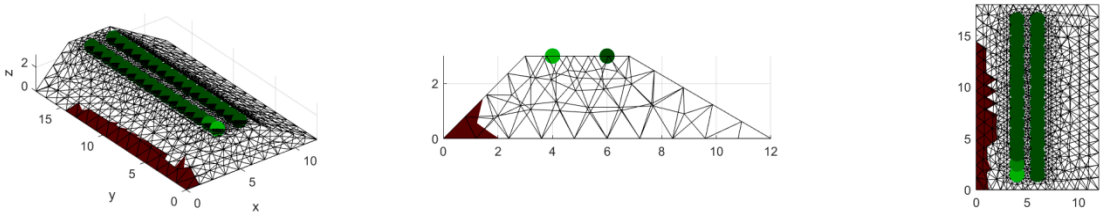

(a)

Preprints (www.preprints.org) | NOT PEER-REVIEWED | Posted: 20 August 2018 doi:10.20944/preprints201808.0346.v1

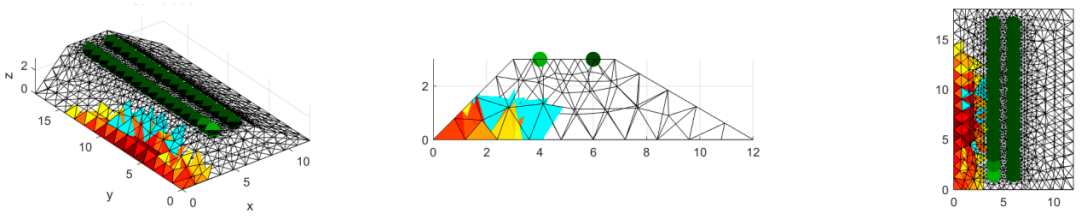

(b)

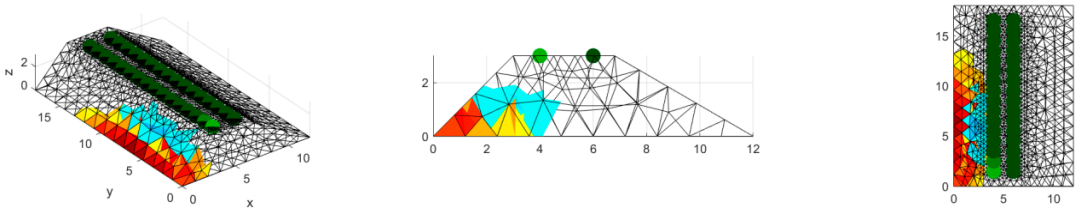

(c)

Figure 27. Model IV flood embankment with 32 electrodes – longer side infiltration of water: (a) pattern, (b) image reconstruction 1, (c) image reconstruction 2

3.5. Image reconfiguration results for Model V

The three-dimensional model V represents a part of the flood embankment. All electrodes are in two planes, which are parallel to the riverbed. This means that in this case the electrodes are arranged along the shaft.

Model parameters:

- number of nodes: 2629,
- number of tetrahedrons: 10,876,
- number of electrodes: 16,
- type of electrodes: points.

For two methods of stimulation (stimulation 1 contains 192 measurements, stimulation 2 contains 96 measurements) the parameters of linear models were estimated using elastic net. The reconstruction results are shown in Fig. 28-30.

Experimental conclusions:

- Increasing the number of measurements visually did not improve the quality of reconstruction.
- Very good reconstruction in case of side seepage of the embankment or a small central one.
- With the help of the V model, reconstructing the depth of seepage of the embankment and permeability length are quite good. It is possible to detect the infiltration that occurs before the nearest plane of electrodes located closest to the riverbed.

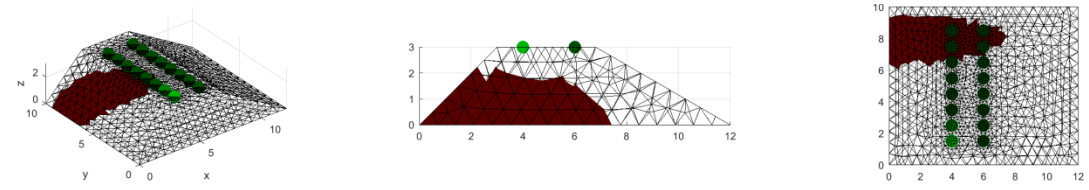

(a)

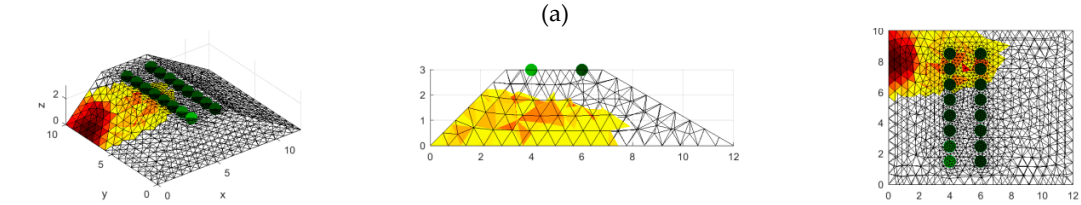

Preprints (www.preprints.org) | NOT PEER-REVIEWED | Posted: 20 August 2018 doi:10.20944/preprints201808.0346.v1

(b)

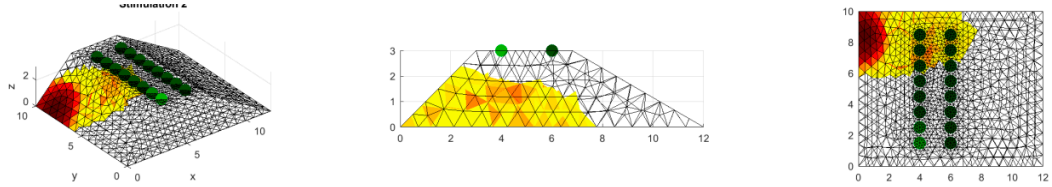

(c)

Figure 28. Model V flood embankment with 16 electrodes – side infiltration of water: (a) pattern, (b) image reconstruction 1, (c) image reconstruction 2

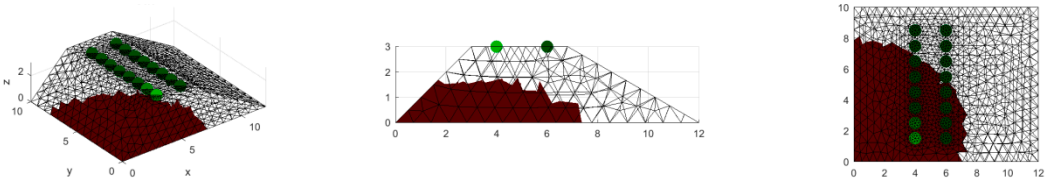

(a)

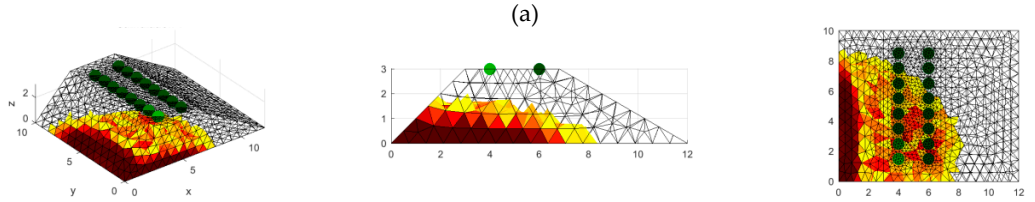

(b)

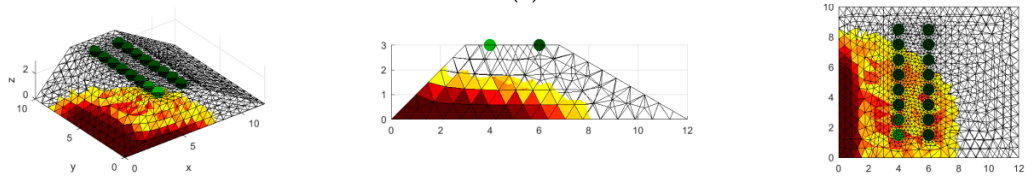

(c)

Figure 29. Model V flood embankment with 16 electrodes – larger side infiltration of water: (a) pattern, (b) image reconstruction 1, (c) image reconstruction 2

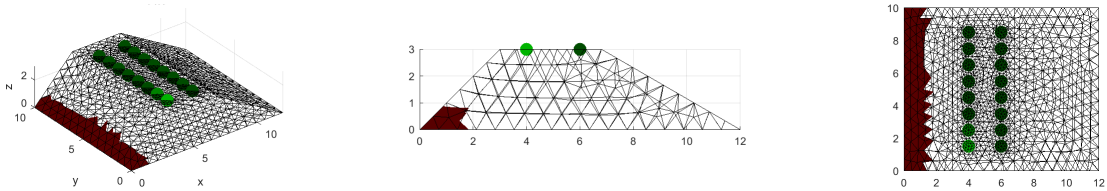

(a)

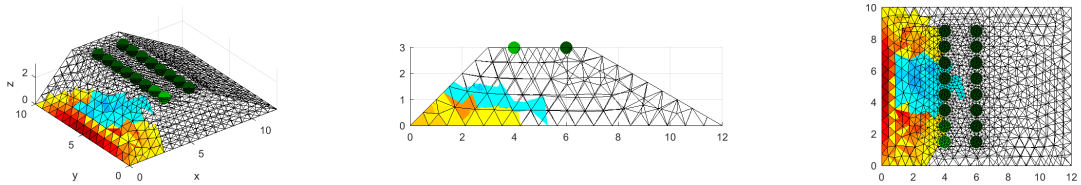

(b)

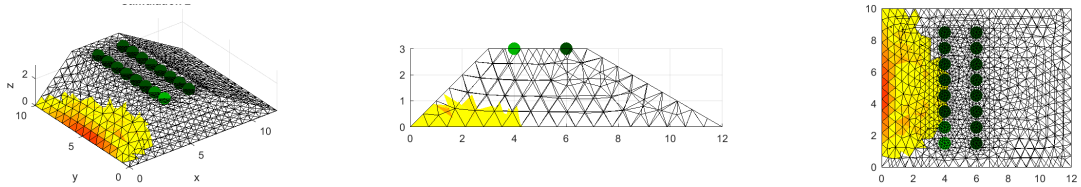

(c)

Preprints (www.preprints.org) | NOT PEER-REVIEWED | Posted: 20 August 2018 doi:10.20944/preprints201808.0346.v1

Figure 30. Model V flood embankment with 16 electrodes – long side infiltration of water: (a) pattern, (b) image reconstruction 1, (c) image reconstruction 2

3.6. Image reconfiguration results for Model VI

The two-dimensional model VI represents the cross section of the flood embankment. All electrodes are placed on the rod and are inserted deeply.

Model parameters:

- number of nodes: 4370,
- number of triangles: 8236,
- number of electrodes: 16,
- type of electrodes: multi-sensors.

For two methods of stimulation (stimulation 1 contains 192 measurements, stimulation 2 contains 96 measurements) the parameters of linear models were estimated using elastic net. The reconstruction results are shown in Fig. 31-33.

Experimental conclusions: reconstruction depends on the learning set.

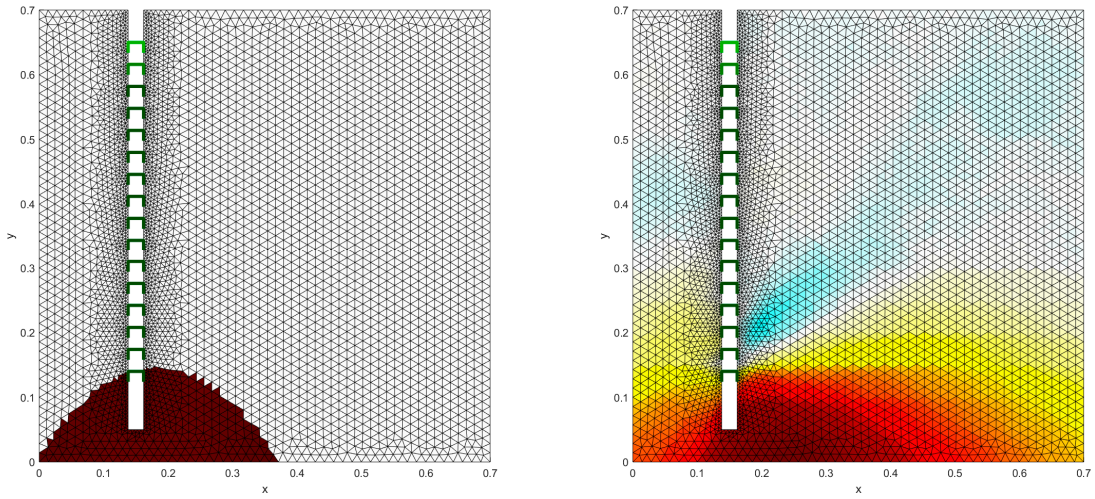

(a) (b)

Figure 31. Model VI flood embankment with 1 multi-sensor electrodes – example I: (a) pattern, (b) image reconstruction

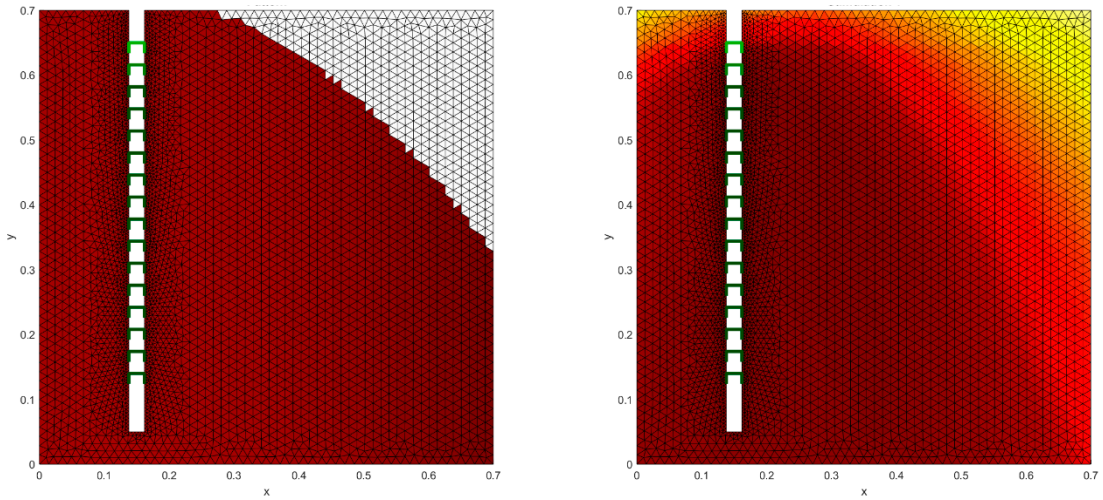

(a) (b)

Figure 32. Model VI flood embankment with 1 multi-sensor electrodes – example II: (a) pattern, (b) image reconstruction

Preprints (www.preprints.org) | NOT PEER-REVIEWED | Posted: 20 August 2018 doi:10.20944/preprints201808.0346.v1

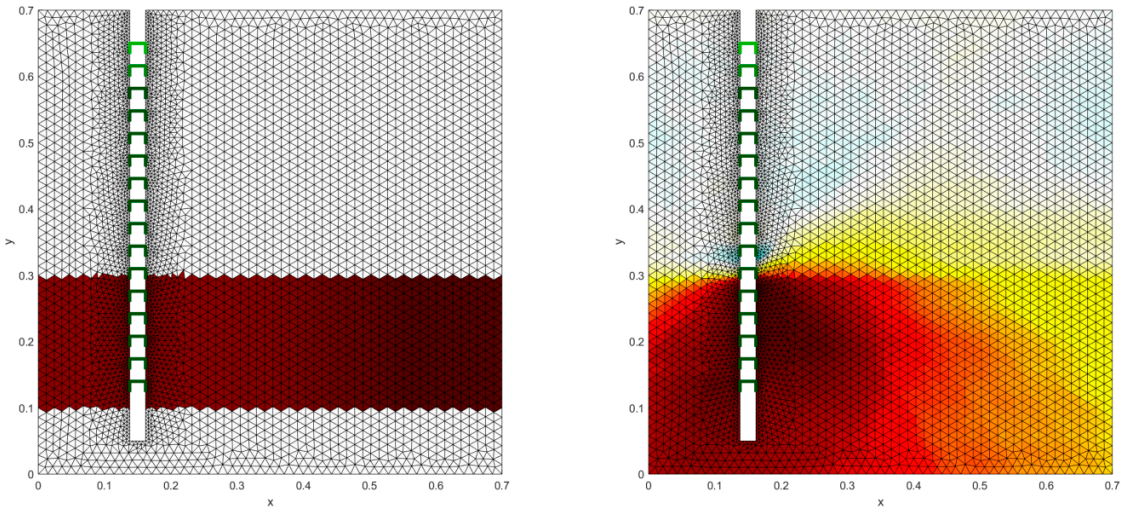

(a) (b)

Figure 33. Model VI flood embankment with 1 multi-sensor electrodes – example III: (a) pattern, (b) image reconstruction

3.7. Image reconfiguration results for Model VII

The two-dimensional model VII represents the cross section of the flood embankment. All electrodes are placed on the rod and are inserted deeply.

Model parameters:

- number of nodes: 6112,
- number of triangles: 11404,
- number of electrodes: 2x16,
- type of electrodes: multi-sensors.

For two methods of stimulation (stimulation 1 contains 896 measurements, stimulation 2 contains 448 measurements) the parameters of linear models were estimated using elastic net. The reconstruction results are shown in Fig. 34-36.

Experimental conclusions: the results for the model VII give more accurate reconstructions compared to the VI model.

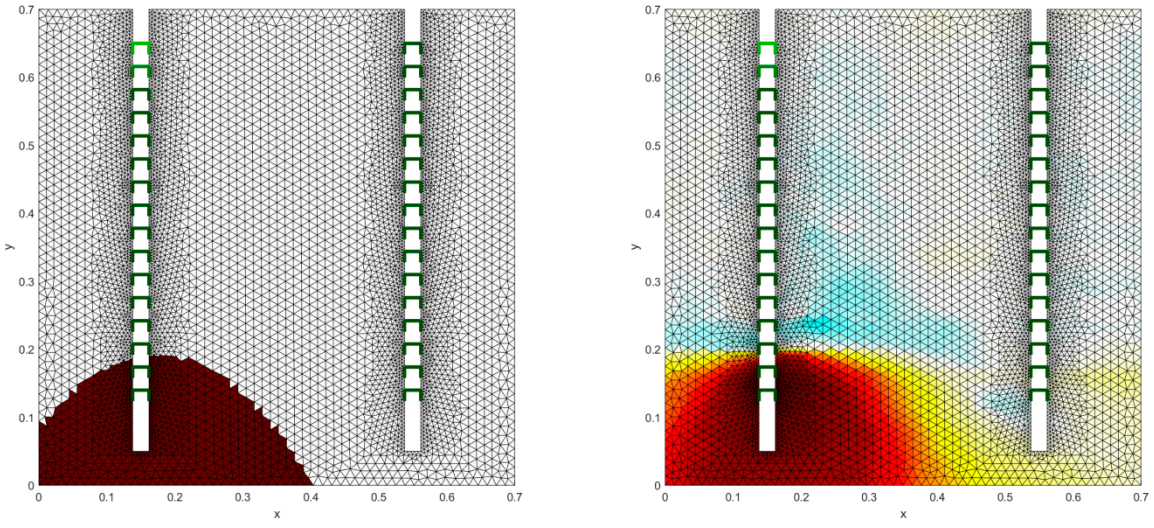

(a) (b)

Figure 34. Model VII flood embankment with 1 multi-sensor electrodes – example I: (a) pattern, (b) image reconstruction

Preprints (www.preprints.org) | NOT PEER-REVIEWED | Posted: 20 August 2018 doi:10.20944/preprints201808.0346.v1

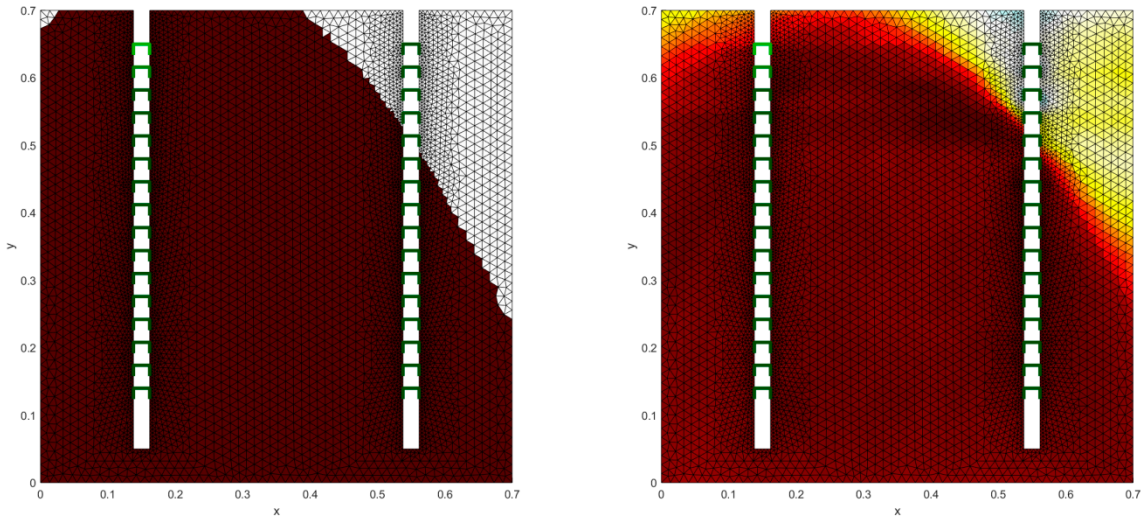

(a) (b)

Figure 35. Model VII flood embankment with 1 multi-sensor electrodes – example II: (a) pattern, (b) image reconstruction

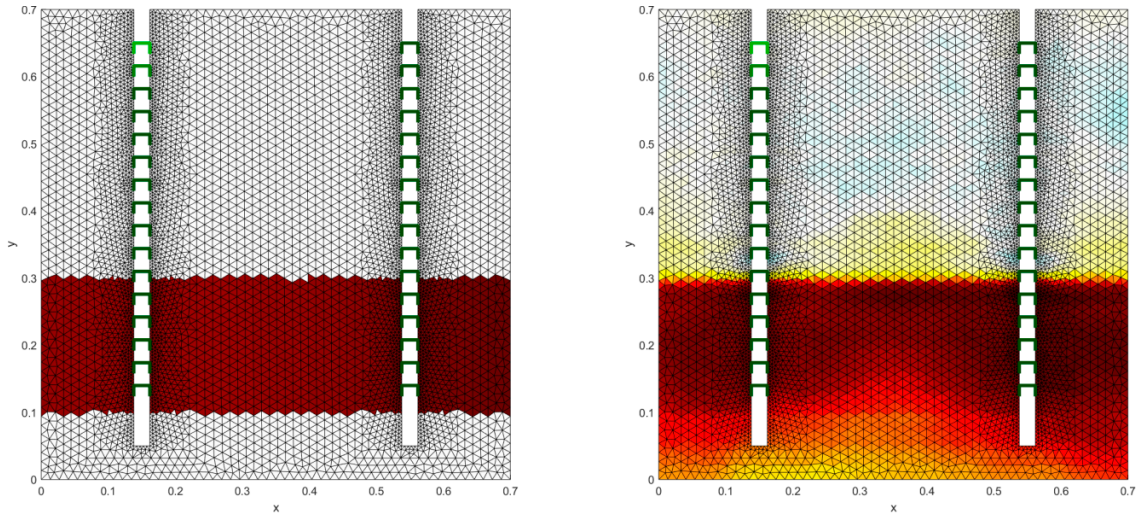

(a) (b)

Figure 36. Model VII flood embankment with 1 multi-sensor electrodes – example III: (a) pattern, (b) image reconstruction

3.8. Test of real object

Figures 37-39 shows the results of the image reconstruction based on real measurements by electrical tomography system.

The three-dimensional model II represents a laboratory fragment of a flood embankment. All electrodes are in two planes.

Model parameters:

- number of nodes: 2991,
- number of tetrahedrons: 12,153,
- number of electrodes: 32,
- type of electrodes: points.

Measurements: 448 voltage.
Reconstruction method: elastic net.
The reconstruction result is shown in Fig. 37.

Preprints (www.preprints.org) | NOT PEER-REVIEWED | Posted: 20 August 2018 doi:10.20944/preprints201808.0346.v1

Experimental conclusions: reconstruction shows area water infiltration.

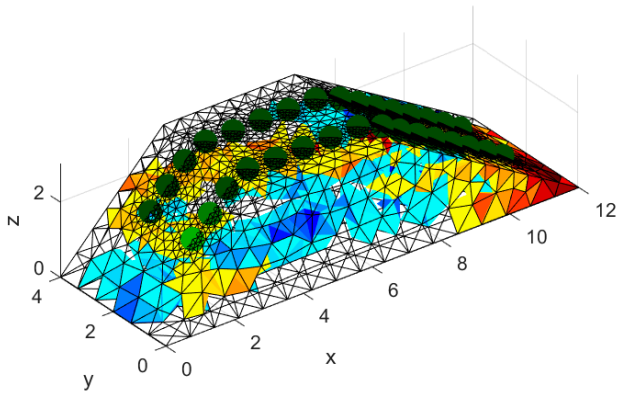

Figure 37. Real reconstruction based on measurement data - model II flood embankment with 32 electrodes

The two-dimensional model VI represents the cross section of the flood embankment. All electrodes are placed on the rod and are inserted deeply.

Model parameters:

- number of nodes: 4370,
- number of triangles: 8236,
- number of electrodes: 16,
- type of electrodes: multi-sensors.

Measurements: 96 voltage.

Reconstruction method: elastic net.

The reconstruction result is shown in Fig. 38.

Experimental conclusions: reconstruction shows area water infiltration.

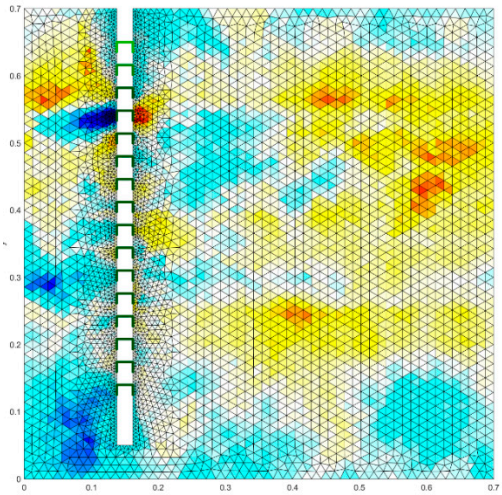

Figure 38. Real reconstruction based on measurement data - model VI flood embankment with 1 multi-sensor electrode

The two-dimensional model VII represents the cross section of the flood embankment. All electrodes are placed on the rod and are inserted deeply.

Model parameters:

- number of nodes: 6112,
- number of triangles: 11404,
- number of electrodes: 2x16,
- type of electrodes: multi-sensors.

Measurements: 448 voltage.

Preprints (www.preprints.org) | NOT PEER-REVIEWED | Posted: 20 August 2018 doi:10.20944/preprints201808.0346.v1

Reconstruction method: elastic net.
The reconstruction result is shown in Fig. 39.
Experimental conclusions: reconstruction shows area water infiltration.

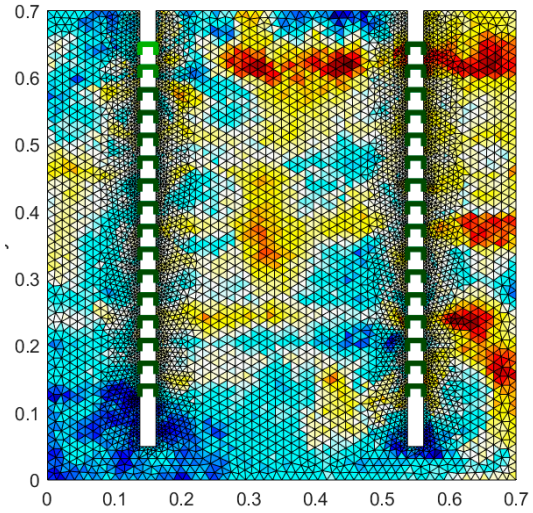

Figure 39. Real reconstruction based on measurement data - model VII flood embankment with 2 multi-sensor electrodes

4. Discussion

4.1. Non-invasive monitoring

Research work presents the original concept of a complex system for monitoring flood embankments. Considering the key design features of this type of solutions and devices, measurement models have been developed to test problems with water leakage and damages in shafts. The models were equipped with a system of point and multi-sensor electrodes and the necessary tomography devices. Such solution allows you to perform many measurements of electrical values, and then their appropriate analysis. The physical processes associated with the failure of the embankment are often complicated and cannot be measured accurately. Such a system can be used as a tool to monitor the embankment in vulnerable conditions. This is an innovative approach, because other methods cannot estimate leaks in the entire volume of the object.

4.2. Technical performance

The presented monitoring system aims to identify changes in flood embankments. The solution determines the level and type of damage (water leaks). The system consists of a set of measuring devices and applications placed in the cloud. Data collected from tomographic devices are transferred to the analytical system. Data processing takes place in real time. The solution is based on a distributed structure for acquisition, processing and analysis of measurement data. The elements of the system include electrical tomograph and auxiliary electric aromas designed and made at Research & Development Centre Netrix S.A. The device measures the tested object based on measurements of the potential distribution, the system collects the measured data from the electrodes. A single device allows measurements up to 32 channels. The devices can work in a distributed system covering the entire examined object.

4.3. Image reconstruction

As part of the work, 7 measurement models were implemented with point and multi-sensor electrodes. The various types and numbers of electrodes were evenly distributed along the boundary and inside of the estimation grid and numerical phantoms. 16 and 32 measuring points are unified with the experimental phantom and its model. The imaging results presented in the previous chapter

show great potential for monitoring the damage. The forward problem was solved by means of the finite element method. To solve the inverse problem, use the elastic net method with ridge and LASSO regularization. Non-linear optimization methods need more time to solve the inverse problem. The presented algorithm after learning works very quickly (the reconstruction time is a fraction of a second). The quality of the resulting images differs when the object is in the middle or near the electrodes located at the border of the domain. It shows reconstructions with sufficient precision. The elastic net gives a rare model with good forecasting accuracy, while encouraging the grouping effect.

4.4. Limitations and future work

Although this research reveals new and promising results, implementation into real objects may be limited by too small quantity of measurement points. The system could be expanded to integrate with other Internet of Things solutions, and the analysis could include a number of different measurement parameters. This work presents a reconstruction based on machine learning (elastic net) algorithms, but the implementation of new methods is unlimited. In the future, the authors plan the development of systems with algorithms related to deep learning and hybrid methods. The design of an electrical tomograph is also developed.

5. Conclusions

The main purpose of the work was to prepare a new technology and an innovative application based on cyber-physical systems and the Internet of Things with the use of electrical impedance tomography to monitor flood embankments. The presented solution enables monitoring of flood embankments in real time. The system allows a visual analysis of damage, which enables quick and effective intervention and possible prevention of danger. The proposed solution includes the analysis of anomalies occurring in the structure of the object as a result of damage or leaks. In this case, it is important to identify the areas at risk of interruption. The main advantage of the application is spatial ability to analyse, high speed of data processing and high accuracy of imaging. Tomography techniques combined with image reconstruction algorithms give a non-invasive and very accurate spatial assessment of water leaks (damages) of flood embankments. This study reveals new and promising results for the practical monitoring of such facilities. In the presented system, a special electronic device was constructed to measure electrical values. The application collects data from such measuring devices and reconstructs images based on them. In order to calculate leaks, algorithms based on elastic net were used to obtain more accurate and stable results of reconstruction in solving the inverse problem in electrical impedance tomography. Prepared numerical models have been successfully used in the system. The presented results show the effectiveness of the research.

Author Contributions: Tomasz Rymarczyk has developed a research project and methods for testing the flood embankment using electrical impedance tomography. As an expert in the work of tomography, he prepared of most concepts of presented techniques in this study. Edward Kozłowski has implemented elastic net method and developed mathematical models' descriptions. Grzegorz Kłosowski carried out research especially in the field of machine learning and analysed objects.

Acknowledgments: The authors would like to thank the authorities and employees of the Institute of Mathematics, Maria Curie-Skłodowska University, Lublin, Poland for sharing supercomputing resources.

Conflicts of Interest: The authors declare no conflict of interest.

References

1. Xu L. D., He W., Li S. Internet of Things in Industries: A Survey, *IEEE Transactions on Industrial Informatics*, **2014**, vol. 10/4, pp. 2233 – 2243, DOI: 10.1109/TII.2014.2300753.
2. Lin J., Yu W., Zhang N., Yang X., Zhang H., Zhao W. A Survey on Internet of Things: Architecture, Enabling Technologies, Security and Privacy, and Applications, *IEEE Internet of Things Journal*, **2017**, vol. 4/5, pp. 1125-1142.

3. Chen F., Deng P., Wan J., Zhang D., Vasilakos A., Rong X. Data Mining for the Internet of Things: Literature Review and Challenges, *International Journal of Distributed Sensor Networks*, **2015**, vol. 12, pp.1-14.
4. Vejar A., Cieplak T., Rymarczyk T. Cloud Computing System for online processing of ERT Data Streams, International Interdisciplinary PhD Workshop 2018, **2018**, Świnoujście, Poland.
5. Holder, D.S. Introduction to biomedical electrical impedance tomography Electrical Impedance Tomography Methods, *History and Applications Bristol: Institute of Physics* **2005**
6. Jones, G.; Sentenac, P.; Zielinski, M. Desiccation cracking detection using 2-D and 3-D Electrical Resistivity Tomography: Validation on a flood embankment. Journal of Applied Geophysics 2014, 106, 196–211.
7. Michta E., Szulim R., Sojka-Piotrowska A., Piotrowski K. IoT based flood embankments monitoring system, Proc. SPIE 10445, Photonics Applications in Astronomy, Communications, Industry, and High Energy Physics Experiments 2017, **2017**, 104455Y, doi: 10.1117/12.2280830.
8. Sekuła K., Połeć M., Borecka A. Innovative solutions in monitoring systems in flood protection, E3S Web of Conferences, Water, Wastewater and Energy in Smart Cities, **2018**, vol. 30, p. 01005, https://doi.org/10.1051/e3sconf/20183001005
9. Forson A., Comas X, Whitman D. Integration of electrical resistivity imaging and ground penetrating radar to investigate solution features in the Biscayne Aquifer, *Journal of Hydrology*, **2014**, vol. 515, pp. 129–138.
10. Beres M., Luetscher M., Olivier R., Integration of ground-penetrating radar and microgravimetric methods to map shallow caves, *Journal of Applied Geophysics*, **2001**, vol. 46, pp. 249–262.
11. De Donno G.; Di Giambattista L.; Orlando, L. High-resolution investigation of masonry samples through GPR and electrical resistivity tomography, *Construction and Building Materials*, **2017**, vol. 154, p. 1234-1249.
12. Bukowska-Belniak B., Borecka A., Leśniak A. The continuous thermal imaging of the flood embankment to identify location of the leaks, 14th Quantitative InfraRed Thermography Conference, 2018.
13. Adler, A.; Lionheart, W. RB. Uses and abuses of EIDORS: an extensible software base for EIT. *Physiological measurement*, **2006**, 27.5: S25.
14. Amaral, M.; Polo, J.; Carrera, D.; Mohomed, I.; Unuvar, M.; Steinder M. Performance evaluation of microservices architectures using containers. Network Computing and Applications (NCA), *2015 IEEE 14th International Symposium on. IEEE*, **2015**, pp. 27–34.
15. Dhamodaran, S.; Sachin, K.; Kumar, R. Big data implementation of natural disaster monitoring and alerting system in real time social network using Hadoop technology, *Indian Journal of Science and Technology*, **2015**, vol. 8/1.
16. Pokrajac, D.; Lazarevic, A.; Latecki, L.J. Incremental local outlier detection for data streams. Computational Intelligence and Data Mining, *CIDM 2007 IEEE Symposium on. IEEE*, **2007**, pp. 504–515.
17. Romanowski A. Big Data-Driven Contextual Processing Methods for Electrical Capacitance Tomography, *IEEE Transactions on Industrial Informatics*, **2018**, p. 1551-3203, DOI: 10.1109/TII.2018.2855200.
18. Sousa, G.; Rudametkin, W.; Duchien, L. Automated setup of multi-cloud environments for microservices applications. Cloud Computing (CLOUD), 9th International Conference on. IEEE, **2016**, pp. 327–334.
19. Karhunen, K.; Seppänen, A.; Kaipio, J. P. Adaptive meshing approach to identification of cracks with electrical impedance tomography, *Inverse Problems & Imaging*, **2014**, vol. 8/1, pp.127-148, doi: 10.3934/ipi.2014.8.127.
20. Filipowicz, S.F.; Rymarczyk, T. The shape reconstruction of unknown objects for inverse problems. *Przeglad Elektrotechniczny*, **2012**, vol. 88, pp. 55–57.
21. Wang M. Industrial Tomography: Systems and Applications, Elsevier, **2015**.
22. Chaniecki K., Romanowski A., Nowakowski J., Niedostatkiewicz M., Application of twin-plane ECT sensor for identification of the internal imperfections inside concrete beams Grudzien, *IEEE Instrumentation and Measurement Technology*, Conference, 2016-July, p. 7520512.
23. Rymarczyk T., Characterization of the shape of unknown objects by inverse numerical methods, *Przeglad Elektrotechniczny*, **2012**, vol. 88/7B, pp. 138-140.
24. Chung, E.T.; Chan, T.F.; Tai, X.C. Electrical impedance tomography using level set representation and total variational regularization. *Journal of Computational Physics*, **2005**, vol. 205, pp. 357–372.
25. Kryszyn J., Smolik W., Olszewski T., Szabatin R., Development of electrical capacitance tomograph design in the nuclear and medical electronics division, *Informatyka, Automatyka, Pomiary w Gospodarce i Ochronie Środowiska (IAPGOŚ)*, **2017**, vol. 7/1, pp. 111-114; DOI: 10.5604/01.3001.0010.4597.
26. Filipowicz, S.F.; Rymarczyk, T. Measurement methods and image reconstruction in electrical impedance tomography. *Przeglad Elektrotechniczny*, **2012**, vol. 88, pp. 247–250.

27. M., Kapusta P., Jackowska-Strumiłło L., Sankowski D. Acceleration of image reconstruction process in the electrical capacitance tomography 3d in heterogeneous, multi-gpu system, *Informatyka, Automatyka, Pomiary w Gospodarce i Ochronie Środowiska (IAPGOŚ)*, **2017**, vol. 7/1, pp. 37-41; DOI: 10.5604/01.3001.0010.4579.
28. Kryszyn J., Wróblewski P., Stosio M., Olszewski T., Smolik W. Architecture of EVT4 data acquisition system for electrical capacitance tomography, *Measurement: Journal of the International Measurement Confederation*, **2017**, vol. 101, pp. 28-39.
29. Majchrowicz M., Kapusta P., Jackowska-Strumiłło L., Sankowski D. Acceleration of image reconstruction process in the electrical capacitance tomography 3d in heterogeneous, multi-gpu system, *Informatyka, Automatyka, Pomiary w Gospodarce i Ochronie Środowiska (IAPGOŚ)*, **2017**, vol. 7/1, pp. 37-41; DOI: 10.5604/01.3001.0010.4579.
30. Banasiak R., Wajman R., Jaworski T., Fiderek P., Fidos H., Nowakowski J. Study on two-phase flow regime visualization and identification using 3D electrical capacitance tomography and fuzzy-logic classification, *International Journal of Multiphase Flow*, **2014**, vol. 58, pp. 1-14.
31. Demidenko, E.; Hartov, A.; Paulsen, K. Statistical estimation of Resistance/Conductance by electrical impedance tomography measurements, *IEEE Transaction on Medical Imaging*, **2004**, vol. 23/7, pp.829-838.
32. Dušek J., Hladký D., Mikulka J. Electrical Impedance Tomography Methods and Algorithms Processed with a GPU, *In PIERS Proceedings*, **2017**, pp. 1710-1714.
33. Rymarczyk, T.; Adamkiewicz, P.; Duda, K.; Szumowski, J.; Sikora, J. New electrical tomographic method to determine dampness in historical buildings, *Archives of Electrical Engineering*, **2016**, vol. 65, pp. 273–283.
34. Garbaa H., Jackowska-Strumiłło L., Grudzień K., Romanowski A. Application of electrical capacitance tomography and artificial neural networks to rapid estimation of cylindrical shape parameters of industrial flow structure, *Archives of Electrical Engineering*, **2016**, vol. 65/4, pp. 657-669.
35. Kryszyn J., Smolik W. Toolbox for 3d modelling and image reconstruction in electrical capacitance tomography, *Informatyka, Automatyka, Pomiary w Gospodarce i Ochronie Środowiska (IAPGOŚ)*, **2017**, vol. 7/1, pp. 137-145; DOI: 10.5604/01.3001.0010.4603.
36. Soleimani M., Mitchell CN, Banasiak R., Wajman R., Adler A., Four-dimensional electrical capacitance tomography imaging using experimental data, *Progress In Electromagnetics Research*, **2009**, vol. 90, pp. 171-186.
37. Hamilton S., Siltanen S. Nonlinear inversion from partial EIT data: computational experiments, *Contemporary Mathematics*, **2014**, vol. 615, pp. 105–129.
38. Rymarczyk T., Kłosowski G., Kozłowski E. Non-Destructive System Based on Electrical Tomography and Machine Learning to Analyze Moisture of Buildings, *Sensors*, **2018**, vol. 18/7, p. 2285.
39. Lechleiter, A.; Rieder, A. Newton regularizations for impedance tomography: convergence by local injectivity. *Inverse Problems*, **2008**, 24(6) 065009.
40. Gunn, D.; Chambers, J.; Uhlemann, S.; Wilkinson, P.; Meldrum, P.; Dijkstra, T.; Haslam, E.; Kirkham, M.; Wragg, J.; Holyoake, S. Moisture monitoring in clay embankments using electrical resistivity tomography, *Construction and Building Materials*, **2015**, vol. 92, pp. 82–94.
41. Voutilainen, A.; Lehikoinen, A.; Vauhkonen, M.; Kaipio, J. Three-dimensional nonstationary electrical impedance tomography with a single electrode layer, *Measurement Science and Technology*, **2010**, vol. 21, p. 035107.
42. Babout L., Grudzień K., Wiącek J., Niedostatkiewicz M., Karpiński B., Szkodo M. Selection of material for X-ray tomography analysis and DEM simulations: comparison between granular materials of biological and non-biological origins, *Granular Matter*, **2018**, vol. 20/3, pp. 20:38.
43. Bartušek K.; Fiala P., Mikulka J. Numerical Modeling of Magnetic Field Deformation as Related to Susceptibility Measured with an MR System, Radioengineering, **2008**, vol. 17/4, pp. 113-118.
44. Rymarczyk, T., Kłosowski, G. Application of neural reconstruction of tomographic images in the problem of reliability of flood protection facilities. *Eksploatacja i Niezawodnosc – Maintenance and Reliability*, **2018**; vol. 20/3, pp. 425–434, http://dx.doi.org/10.17531/ein.2018.3.11.
45. Bartusek K., Kubasek R., Fiala P. Determination of pre-emphasis constants for eddy current reduction, *Measurement science and technology*, **2010**, vol. 21/10, p. 105601.
46. Kłosowski G., Kozłowski E., Gola A., Integer linear programming in optimization of waste after cutting in the furniture manufacturing, *Advances in Intelligent Systems and Computing 2018;* **2018**, vol. 637, pp. 260-270.

47. Kosicka E., Kozłowski E., Mazurkiewicz D. Intelligent Systems of Forecasting the Failure of Machinery Park and Supporting Fulfilment of Orders of Spare Parts, *Intelligent Systems in Production Engineering and Maintenance – ISPEM 2017*, 2018, pp. 54–63.
48. Polakowski K., Filipowicz S.F., Sikora J., Rymarczyk T. Tomography Technology Application for Workflows of Gases Monitoring in the Automotive Systems, *Przeglad Elektrotechniczny*, **2008**, vol. 84/12, pp. 227-229.
49. Lopato P., Chady T., Sikora R., Ziolkowski S., M. Full wave numerical modelling of terahertz systems for nondestructive evaluation of dielectric structures, *COMPEL - The international journal for computation and mathematics in electrical and electronic engineering*, **2013**, vol. 32/3, pp. 736 – 749.
50. Mazurkiewicz D. Maintenance of belt conveyors using an expert system based on fuzzy logic, *Archives of Civil and Mechanical Engineering*, **2015**; vol. 15/2, pp. 412-418.
51. Othman, M.F.; Shazali, K. Wireless sensor network applications: A study in environment monitoring system, *Procedia Engineering*, **2012**, vol. 41, pp. 1204–1210.
52. Psuj G. Multi-Sensor Data Integration Using Deep Learning for Characterization of Defects in Steel Elements, *Sensors*, vol. 18/1, **2018**, p. 292; https://doi.org/10.3390/s18010292.
53. Ziolkowski M., Gratkowski S., Zywica A. R., Analytical and numerical models of the magnetoacoustic tomography with magnetic induction, *COMPEL - The international journal for computation and mathematics in electrical and electronic engineering*, **2018**, vol. 37/2, pp. 538–548.
54. Prato M., Zanni L., Inverse problems in machine learning: An application to brain activity interpretation, *Journal of Physics: Conf. Ser.*, 2008, 135 012085.
55. Lee Y., Nguyen V., Wang D., On Variable and Grouped Selections of the Elastic Net, Report CS532, **2016**, pp. 1–24.
56. Zou, H., Hastie, T. Regularization and variable selection via the elastic net. *Journal of the Royal Statistical Society*, Series B, **2005**, vol./2, pp. 301–320.
57. Tibshirani, R. Regression shrinkage and selection via the lasso, Journal of the Royal Statistical Society, Series B, **1996**, vol. 58/1, pp. 267–288.
58. Wehrens R.: Chemometrics with R. Multivariate Data Analysis in the Natural Science and Life Sciences, Springer, **2011**.
59. Xin Yan, Xiao Gang Su: Linear regression analysis: Theory and computing, *World Sciencific*, **2009**.
60. Hastie, T.; Tibshirani, R.; Friedman, J. The Elements of Statistical Learning Data Mining, Inference, and Prediction, Springer, New York, **2009**.
61. James, G.; Witten, D.; Hastie, T.; Tibshirani, R. *An Introduction to Statistical Learning with Applications in R*, Springer, New York, **2013**.